PCAF-mediated histone acetylation promotes replication fork degradation by MRE11 and EXO1 in BRCA-deficient cells

Jae Jin Kim[1,5], **Seo Yun Lee**[1,5], **Ji-Hye Choi**[3], **Hyun Goo Woo**[3,4], **Blerta Xhemalce**[1,2], **Kyle M. Miller**[1,2,6,*]

[1]Department of Molecular Biosciences, The University of Texas at Austin, Austin, TX 78712, U.S.A.

[2]Livestrong Cancer Institutes, Dell Medical School, The University of Texas at Austin, Austin, TX 78712, U.S.A.

[3]Department of Physiology, Ajou University School of Medicine, Suwon, 16499, Republic of Korea

[4]Department of Biomedical Science, Graduate School, Ajou University, Suwon, 16499, Republic of Korea

[5]These authors contributed equally

[6]Lead Contact

SUMMARY

Stabilization of stalled replication forks is a prominent mechanism of PARP inhibitor (PARPi) resistance in *BRCA*-deficient tumors. Epigenetic mechanisms of replication fork stability are emerging but remain poorly understood. Here, we report the histone acetyltransferase PCAF as a fork-associated protein that promotes fork degradation in BRCA-deficient cells by acetylating H4K8 at stalled replication forks, which recruits MRE11/EXO1. The H4K8ac binding domain of MRE11/EXO1 are required for their recruitment to stalled forks. Low PCAF levels, which we identify in a subset of *BRCA2*-deficient tumors, stabilize stalled forks resulting in PARPi resistance in BRCA-deficient cells. Furthermore, PCAF activity is tightly regulated by ATR, which phosphorylates PCAF on S264 to limit its association and activity at stalled forks. Our results reveal PCAF and histone acetylation as critical regulators of fork stability and PARPi responses in BRCA-deficient cells, which provides key insights into targeting *BRCA*-deficient tumors and identifying epigenetic modulators of chemotherapeutic responses.

*Correspondence: kyle.miller@austin.utexas.edu (K.M.M.), Telephone: 001 512 471-5045; Fax: 001 512 373-3800.

In Brief

Kim et al. demonstrate replication fork association of the histone acetyltransferase PCAF, which promotes replication fork degradation in BRCA-deficient cells. Nucleases MRE11 and EXO1 bind PCAF-mediated H4K8ac at stalled forks. PCAF loss confers PARP inhibitor resistance in BRCA-deficient cells, identifying PCAF and H4K8ac in chemotherapeutic responses and fork stability.

Graphical Abstract
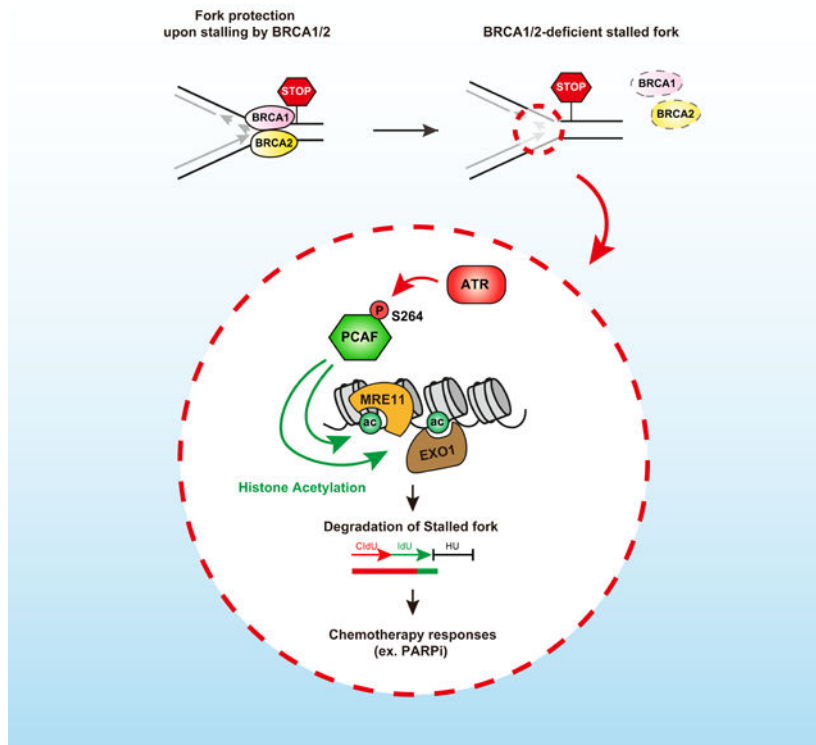
Keywords

Acetylation; Bromodomain; BRCA1 and BRCA2; PCAF; PARP; Replication fork stability; MRE11; EXO1; DNA replication stress

INTRODUCTION

Genomic instability is a key contributor to tumorigenesis in many cancers (Hanahan and Weinberg, 2011; Negrini et al., 2010). BRCA1 and BRCA2 are important tumor suppressors that regulate homologous recombination repair (HR) to maintain genome stability (Gudmundsdottir and Ashworth, 2006). Germline or somatic mutations in *BRCA1/2* are associated with increased risk of breast, ovarian and other cancers (Couch et al., 2014; King, 2014). BRCA1/2 regulate several steps in HR, including inhibiting 53BP1 to activate DNA-end resection and orchestrating the loading of the recombinase RAD51 onto resected DNA, a key step in HR-mediated DNA repair. BRCA1/2 also protect stalled replication forks from

degradation. Upon fork stalling, fork reversal can occur and nascent DNA strands upon fork reversal are degraded by DNA nucleases in cells deficient for BRCA1/2 (Lemacon et al., 2017; Porro et al., 2017; Quinet et al., 2017b; Rondinelli et al., 2017; Schlacher et al., 2011; Schlacher et al., 2012; Thangavel et al., 2015; Ying et al., 2012). CtIP facilitates fork degradation by the nucleases MRE11 and EXO1, leading to substrates for MUS81-mediated cleavage of regressed forks in BRCA-deficient cells (Lemacon et al., 2017). BRCA1/2 are thought to protect reversed forks through the stabilization of RAD51 in a HR-independent pathway.

PARP inhibitors (PARPi) represent one of the most promising treatments for *BRCA*-mutated cancers. PARPi affect HR and replication fork stabilization in BRCA-deficient cells (Bast et al., 2009; Bryant et al., 2005; Farmer et al., 2005; Kennedy and D'Andrea, 2006). PARP inhibitors (ex. Olaparib) act by trapping PARP onto DNA during replication. PARP trapping impedes progression of replication causing replication fork collapse in the absence of BRCA1/2 (Hopkins et al., 2015; Murai et al., 2012; Murai et al., 2014; Pettitt et al., 2013). These cells undergo programmed cell death or attempt to repair by non-homologous end-joining (NHEJ), which may cause gross genomic instability (Lord and Ashworth, 2012).

Although PARPi are FDA approved in some cancer settings, drug resistance and tumor relapse are common. Several mechanisms of PARPi resistance have been identified (Lord and Ashworth, 2012; Noordermeer and van Attikum, 2019; Ray Chaudhuri et al., 2016). One PARPi resistance mechanism involves the loss of HR repair antagonizing proteins (e.g. 53BP1 and Rev7) (Jaspers et al., 2013; Xu et al., 2015), restoring HR even with mutated *BRCA1*. Another resistance mechanism involves replication fork stabilization by PTIP or EZH2 depletion (Ray Chaudhuri et al., 2016; Rondinelli et al., 2017). Upon PTIP or EZH2 deficiency, replication forks are stabilized due to the failed recruitment of DNA nucleases, including MRE11 or MUS81. Histone methylation by PTIP-MLL3/4 (i.e. H3K4me1/3) and EZH2 (i.e. H3K27me3) promotes MRE11 and MUS81 recruitment to replication forks, respectively (Ray Chaudhuri et al., 2016; Rondinelli et al., 2017). Chromatin remodeling activities including from FANCD2 and CHD4 also participate in replication fork processing (Guillemette et al., 2015; Higgs et al., 2018; Ray Chaudhuri et al., 2016). Thus, histone methylation, and perhaps other histone modifications and chromatin regulators, are vital participants in replication fork stability. Identification of mechanisms involved in protecting replication forks in BRCA-deficient cells is important as they can inform on the efficacy of PARPi therapies and predict *BRCA*-deficient tumor responses.

Histone acetylation is essential for genome integrity, replication and the DNA damage response (DDR) (Gong et al., 2016; Kim et al., 2019c; MacAlpine and Almouzni, 2013). Histone acetylation provides signals on chromatin that are recognized by histone acetylation reader proteins. For example, bromodomain proteins recognize acetylated histones *via* their bromodomain (BRD), an evolutionary conserved domain that binds acetylated lysines (Dhalluin et al., 1999; Filippakopoulos et al., 2012). Humans encode 42 BRD proteins, which play important roles in transcription, chromatin remodeling and DNA repair (Fujisawa and Filippakopoulos, 2017; Gong et al., 2016; Kim et al., 2019b). Recent studies identified bromodomain-containing protein 4 (BRD4) as a synthetic lethal target in conjunction with PARPi (Sun et al., 2018; Yang et al., 2017). BRD4 inhibition reduced HR

in BRCA proficient cancers by repressing the transcription of *BRCA1*, *RAD51* (Yang et al., 2017), and *CtIP* (Sun et al., 2018). The lysine acetyltransferase 2B, KAT2B (commonly known as PCAF), acetylates core histones to promote transcription activation (Ogryzko et al., 1996) and is involved in DNA repair including HR (Clouaire et al., 2018; He et al., 2017; Kim et al., 2019b; Zhao et al., 2017). For instance, PCAF induces H2BK120 acetylation at DNA double-strand breaks (DSBs) to facilitate HR (Clouaire et al., 2018; Kim et al., 2019b; Li et al., 2018). Although over half of human BRD proteins participate in DSB repair (Chiu et al., 2017; Gong et al., 2015; Kim et al., 2019b), little is known about their functions in DNA replication. How these proteins, along with histone acetylation, impact PARPi sensitivity in *BRCA*-deficient cancers is also unclear.

In this study, we find that among human BRD proteins, PCAF uniquely exhibited reduced expression in *BRCA2*-mutated cancers, which prompted an evaluation of PCAF in replication including fork stability. We identified PCAF as a replication fork-associated protein and PCAF-mediated histone acetylation as a key signaling event for replication fork stability in BRCA-deficient cells. PCAF promotes degradation of stalled replication forks by acetylating histone H4 at lysine 8 (H4K8ac). This mark promotes the recruitment of MRE11 and EXO1 to stalled replication forks. We also determined that ATR, an important replication stress kinase, phosphorylates PCAF on serine 264, to suppress excessive recruitment of PCAF to replication forks to prevent fork degradation. Collectively, our data identifies PCAF and histone acetylation as vital components of replication fork stabilization mechanisms that impact PARPi responses in BRCA-deficient cells.

RESULTS

PCAF gene expression is down regulated in *BRCA2*-mutated breast cancer.

Previous strategies using gene expression profiles in HR-deficient tumors have identified regulators involved in chemotherapeutic responses in *BRCA*-deficient tumors (Rondinelli et al., 2017). To investigate the potential importance of BRD proteins in *BRCA*-mutant cancers, we analyzed the expression of BRD genes in *BRCA*-deficient tumors using published data from The Cancer Genome Atlas (TCGA) breast cancer consortium (http://www.cbioportal.org) and STAR Methods). Among 39 human BRD genes that are broadly expressed, several exhibited significant alterations in expression in *BRCA1/2*-mutated cancers. In *BRCA1* and *BRCA2*-mutated cancers, *ATAD2* levels are increased, while *PCAF* expression is highly reduced in BRCA2-mutated breast cancers (Figures 1A and 1B; Figure S1A). Analysis of PCAF protein and mRNA levels in several model breast cancer cell lines yielded similar results when comparing several *BRCA*-mutated versus WT *BRCA1/2* breast cancer cell lines (Figures S1B and S1C). We also analyzed overall survival in these cancers as it relates to *PCAF* expression levels. While separating *PCAF* high-or low-expressed cohorts in BRCA2-mutated breast cancers was not infeasible due to overall low *PCAF* expression (Figure 1B), these cohorts were obtainable in *BRCA1/2*-mutated ovarian cancer patient samples since *PCAF* expression was more widely distributed (Figures S1D–S1F). *BRCA2*-mutated ovarian cancers with low *PCAF* expression displayed poor overall survival compared to those with high *PCAF* expression, with a similar trend indicated in *BRCA1*-mutated ovarian cancers (Figure S1D). No difference in overall survival probability in low

and high *PCAF* expressing cohorts in *BRCA1/2* WT ovarian cancers was observed (Figure 1SD). These results reveal reduced *PCAF* levels in *BRCA2*-deficient tumors and provide evidence for clinical relevance of these observations.

PCAF contributes to PARP inhibitor sensitivity in BRCA-deficient cells.

Given the potential relationship and clinical relevance of *PCAF* levels in BRCA2-deficient tumors and cells (Figures 1A–B and S1B–D), we hypothesized that PCAF may impact HR and chemotherapeutic responses in BRCA-mutated cells. To test this hypothesis, we evaluated PARPi sensitivity in BRCA1/2 and PCAF co-depleted cells (Figures 1C–1E). As expected, depletion of BRCA1/2 in U2OS osteosarcoma cancer cells resulted in PARPi sensitivity. PCAF-depleted cells were mildly sensitive to PARPi, consistent with its known role in HR (Kim et al., 2019b). Importantly, PCAF loss promoted resistance to PARPi treatment in BRCA1- or BRCA2-depleted U2OS cells (Figures 1C and 1D). We further assessed PARPi resistance in the *BRCA2*-mutated ovarian adenocarcinoma cancer cell line PEO1. Consistent with results in U2OS cells, PCAF-depleted PEO1 cells enhanced PARPi resistance compared to *BRCA2*-proficient PEO4 cells, confirming these results and ruling out any cell line specific effects (Figure 1E).

One mechanism for PARPI resistance in BRCA-deficient cells is restoration of HR repair, which has been shown for 53BP1 loss (Bouwman et al., 2010). This mechanism is unlikely to explain why PCAF loss promotes PARPi resistance in BRCA1/2-deficient cells due to the following observations. PCAF loss alone results in HR deficiency and double knockdown of PCAF and BRCA1 or BRCA2 did not alter the already reduced HR efficiency in BRCA1/2 defective cells (Figures 1F and S1G; 53BP1 is a positive control for rescue of HR-deficiency in BRCA1-deficient cells). Similar results were obtained when we analyzed foci formation of the HR factor RAD51 after ionizing radiation (IR, 5 Gy). RAD51 binds single-stranded endresected DNA during HR repair. Unlike the known restoration of RAD51 foci in 53BP1 and BRCA1 co-depleted cells (Nacson et al., 2018), depletion of PCAF in BRCA1/2 did not rescue RAD51 accumulation at damage sites in IR-treated cells (Figure 1G), strongly suggesting HR restoration is not involved in PCAF-mediated PARPi resistance in BRCA-deficient cells.

PCAF localizes to stalled replication forks and promotes their degradation in BRCA-deficient cells.

In addition to HR repair, BRCA1/2 also regulates replication fork stability during replication stress (Schlacher et al., 2011; Schlacher et al., 2012). In the absence of BRCA1/2, nascent DNA at the replication fork is extensively degraded by DNA nucleases (Lemacon et al., 2017; Ying et al., 2012). Replication fork stability contributes to PARP inhibitor responses in BRCA-deficient cells (Liao et al., 2018; Noordermeer and van Attikum, 2019; Ray Chaudhuri et al., 2016; Rondinelli et al., 2017; Taglialatela et al., 2017). To investigate a role for PCAF in replication fork protection, we performed DNA fiber assays using 5-Chloro-2'-deoxyuridine (CIdU) and 5-Iodo-2'-deoxyuridine (IdU) thymidine analog labeling followed by hydroxyurea (HU) treatment, which induces replication stress. Unlike siControl (siCtrl) cells, BRCA1- or BRCA2-depleted cells displayed a diminished ratio of IdU/CIdU tracts, which is indicative of fork degradation (Figure 2A; Figure 2B validates siRNA-dependent

protein depletion). PTIP (MLL3/4 complex protein) loss protects stalled replication forks in BRCA-deficient cells, by inhibiting MRE11-dependent degradation and was used as a positive control for fork protection in BRCA1- and BRCA2-depleted cells (Ray Chaudhuri et al., 2016). Cells depleted for PCAF displayed mild fork instability compared to siCtrl cells, which was not associated with aberrant fork progression as a result of PCAF-deficiency (Figure S2A). Similar to PTIP, PCAF depletion resulted in suppression of fork degradation in BRCA-deficient cells (Figures 2A and 2B). These results suggest that PCAF is involved in promoting fork degradation specifically in BRCA-deficient cells.

To investigate if PCAF acted directly at stressed replication forks, we examined PCAF localization at stalled replication forks using a Lac operon array (LacO×256) system that is stably integrated into U2OS-LacO-I-SceI-TetO cell line (Figure 2C). Binding of Lac repressor (LacR) to LacO arrays acts as a replication barrier, resulting in localized replication fork stalling and DNA damage in S-phase (Beuzer et al., 2014; Kim et al., 2018). Using mCherry-tagged LacR to visualize binding to this locus, recruitment of endogenous PCAF to mCherry-LacR bound LacO arrays was observed (Figure 2C). To assess PCAF localization at replication forks more directly, we employed Isolation of Proteins On Nascent DNA (iPOND), a robust technique capable of identifying replication fork-associated proteins (Dungrawala and Cortez, 2015; Rondinelli et al., 2017). iPOND revealed that endogenous PCAF accumulated on newly replicated DNA and disappeared following thymidine chase (Figure 2D). PCNA, a known replication fork associated protein acted as a positive control. Upon HU-induced replication stress, we observed enrichment of PCAF by iPOND in HU-treated samples (Figure 2E). To better quantify these results, we used SIRF assay (*in situ* protein interactions at nascent and stalled replication forks), which uses proximity ligation assay (PLA) technology (Figure S2B) (Roy et al., 2018). Using this assay, enrichment of PCAF at stalled replication forks was also detected (Figure S2C). These data establish that PCAF is a replication fork-associated protein, including after replication stress.

PCAF has three functional domains including the N-terminal (1–320), central N-acetyltransferase (N-AT, 503–651) and the C-terminal bromodomain (BRD, 740–832). To specify critical regions of PCAF involved in replication, we generated PCAF deletion mutants of these regions (N,   N-AT and   C; Figure S2D) and tested their ability to translocate to stalled replication forks using the U2OS-LacO–/–ISceI-TetO cell line. The N-terminal domain of PCAF was required for recruitment, while both the HAT and BRD domains were dispensable (Figures 2F and S2E). These results were validated by iPOND, which revealed that WT but not   N of GFPPCAF localized to replication forks (Figure 2G). Thus, PCAF utilizes its N-terminal domain to localize to replicating DNA, independently of its acetylation and acetyllysine binding capabilities.

PCAF recruits MRE11 and EXO1 to promote degradation of stalled replication fork in BRCA-deficient cells

We next set out to determine the molecular mechanism of PCAF-dependent fork degradation in BRCA-deficient cells. A number of DNA nucleases process stalled forks (Lemacon et al., 2017; Mijic et al., 2017; Porro et al., 2017; Quinet et al., 2017b; Rondinelli et al., 2017; Thangavel et al., 2015). Therefore, we investigated whether PCAF cooperates with specific

DNA nucleases to promote replication fork degradation. To address this question, we performed DNA fiber assays in cells overexpressing PCAF. While PCAF overexpression did not affect fork stability after HU-treatment in WT cells, cells deficient for BRCA1 or BRCA2 displayed reduced IdU tracks (i.e. fork degradation) as expected (Figures 3A, 3B, S3A and S3B). Interestingly, overexpression of PCAF was able to further reduce IdU tracks in both BRCA1- and BRCA2-deficient cells (Figures 3A, 3B, S3A and S3B). Using this observation to assess fork degradation, we found that out of 6 DNA nucleases tested, only MRE11 and EXO1 knockdown reverted fork degradation induced by overexpression of PCAF in BRCA1/2-deficient cells (Figures 3A and 3B; S3A and S3B). These results point to a connection between PCAF and these nucleases in fork degradation in BRCA1/2-deficient cells.

Upon identifying MRE11 and EXO1 in PCAF-mediated fork degradation in BRCA-deficient cells, we sought to determine whether PCAF is required for their recruitment to stalled replication forks. To this end, we quantified MRE11 and EXO1 localization at stalled replication forks using several independent assays; LacO array system, SIRF assay and iPOND. Depletion of PCAF decreased MRE11 and EXO1 recruitment to stalled replication forks as assayed by recruitment to LacO following LacR expression (Figures S4A and S4B), SIRF assay in BRCA1- or BRCA2-deficient cells treated with EdU and HU (Figures 3C, 3D, S4C and S4D) and iPOND samples upon HU-treatment (Figure 3E). The requirement for PCAF in MRE11 and EXO1 recruitment to stressed forks appeared to be damage specific, as depletion of PCAF had no discernable effect on the recruitment of either nuclease to laser-induced DNA damage (Figures S4E and S4F). The histone methyltransferase EZH2 promotes the degradation of stalled replication forks by recruiting the nuclease MUS81 (Rondinelli et al., 2017). EZH2 accumulation on stalled forks was not affected in PCAF-deficient cells, suggesting that these results were independent of EZH2 and that multiple chromatin-modification pathways participate in fork degradation at stalled replication forks (Figure 3E).

Given that PCAF, MRE11 and EXO1 are recruited to stalled replication forks, we postulated that these factors may interact. To test this idea, we performed co-immunoprecipitation experiments, which revealed an interaction between PCAF and both MRE11 and EXO1, using both exogenously expressed GFP-tagged proteins and under endogenous protein expression conditions (Figures S4G–S4J). Interestingly, these interactions were enhanced under conditions of replication stress (i.e. HU, Figures S4G–S4I). These data demonstrate that PCAF is a replication fork associated protein that promotes MRE11 and EXO1 recruitment to stalled replication forks.

MRE11 and EXO1 bind to H4K8ac

PCAF has several functional domains, which could mediate both its fork degradation promoting activities (Figure S2D). To determine how PCAF regulates MRE11- and EXO1-mediated fork degradation, we utilized PCAF KO cells complemented with various PCAF mutants. While BRCA2-deficiency resulted in fork degradation that was suppressed in PCAF KO cells, ectopic expression of full-length PCAF was able to rescue this phenotype (Figures S5A and S5B). These results not only validate that this phenotype is due to the

specific loss of PCAF in PCAF KO cells, but also provide a robust complementation assay to assess the specific region(s) of PCAF involved in promoting fork degradation. Using this complementation assay, we determined that the N-terminal and N-Acetyltransferase (N-AT) domains of PCAF are required for fork degradation in BRCA2-deficient cells, while the BRD of PCAF is dispensable (Figures S5A and S5B). While the involvement of the N-terminal domain of PCAF was expected, as we had identified this region as being important for recruitment to replication forks (Figures 2F and 2G), the involvement of the N-AT domain suggests that the acetyltransferase activity of PCAF is involved in fork degradation promotion as well.

To further support this idea, we engineered a catalytically-dead PCAF mutant by introducing two missense mutations YF to AA in N-AT (PCAF-YFAA), which abolishes histone acetyltransferase activity in PCAF (Clements et al., 1999; Kim et al., 2019b). Consistent with our data obtained using the N-AT domain deletion mutant of PCAF expressed in PCAF KO cells (Figures S5A and S5B), catalytically dead PCAF-YFAA was unable to rescue fork degradation in BRCA2-deficient cells (Figure 4A). We also tested for PARPi sensitivity, which correlates with replication fork stability. While depletion of BRCA2 resulted in PARPi sensitivity compared to WT U2OS cells, PCAF deletion by CRISPR-Cas9 in U2OS cells led to PARPi resistance in BRCA2-depleted cells (Figures S5C and S5D). PARPi resistance was reverted by expression of WT PCAF but not PCAF-YFAA. These data indicate that the HAT activity of PCAF is required for MRE11 and EXO1 dependent fork degradation in BRCA2-deficient cells, which modulates PARPi responses in these cells.

Recent studies identified the involvement of histone methylations on H3 in DNA nuclease recruitment to replication forks (Ray Chaudhuri et al., 2016; Rondinelli et al., 2017). We hypothesized that PCAF may regulate MRE11 and EXO1 recruitment through histone acetylation. To test this hypothesis, we performed binding studies with recombinant MRE11/RAD50 and EXO1 to a large assortment of histone modifications using Modified Histone peptide Array™ analyses. Using this assay, we observed that MRE11/RAD50 and EXO1 proteins exhibited increased binding to histone H4K8 acetyl-peptides (H4K8ac) (Figure 4B). We next validated these interactions using biotinylated H4K8ac peptides in cells. Consistent with the observed binding of H4K8ac within the modified histone peptide array, endogenous and recombinant MRE11 and EXO1 both exhibited enhanced binding to H4K8ac peptides compared to unmodified H4 (Figures 4C and S6A).

We next set out to identify which domain within MRE11 and EXO1 was responsible for H4K8ac binding, since these proteins do not contain a canonical acetyl-lysine binding domain (e.g. BRD). Using sequential C-terminal deletions for MRE11 and EXO1, we performed H4K8ac peptide pull-down assays from cells expressing these derivatives. While we could readily pull-down MRE11 and EXO1 with H4K8ac peptides, these interactions were dependent on MRE11 407–555 and EXO1 1–137 regions (Figures S6B and S6C). To map the precise interaction domain, additional mutations within these putative binding domains of MRE11 and EXO1 were generated (Figures 4D and 4E). Using these small deletions, acetylated H4K8 binding to MRE11 and EXO1 were mapped to MRE11 (Δ1:a.a. 407–421) and the PIN domain of EXO1 (a.a. 125–135) (Figures 4D and 4E). Interestingly, previous studies have suggested that both of these regions in MRE11 (a.a. 407–421) and

EXO1 (PIN; a.a. 125–135) are involved in nucleic acid interactions (Arcus et al., 2011; Glavan et al., 2006; Stracker and Petrini, 2011). However, peptide pull-down experiments were performed with Turbo nuclease to exclude interactions mediated by nucleic acids. Furthermore, interactions were observed specifically with H4K8ac and not unmodified H4 peptide, which has an additional positive charge that could interact with DNA (Figures 4C–4E, S6B and S6C). Recombinant MRE11 and EXO1 exhibited direct interactions with H4K8ac containing peptides in *in vitro* conditions lacking nucleic acids (Figure S6A). In support of histone acetylation of PCAF driving replication fork interactions of MRE11 and EXO1, both the MRE11 1 and EXO1 PIN did not accumulate at replication forks (Figures 4F and 4G). These data suggest that MRE11 and EXO1 bind H4K8ac to promote recruitmentto replication forks.

PCAF acetylates H4K8 to recruit MRE11 and EXO1 to replication forks.

Given that PCAF is required for MRE11 and EXO1 recruitment to replication forks and that MRE11 and EXO1 bind to H4K8ac (Figures 3 and 4), we postulated that PCAF directly acetylates H4 at lysine 8. To address this question, we performed *in vitro* acetylation assays using purified PCAF (Kim et al., 2019b). Indeed, we observed that PCAF could directly acetylate H4 on K8, which was dependent on its acetylase activity (Figures 5A and 5B; Note: H4K8ac levels are lost in the PCAFYFAA mutant). We next assessed H4K8 acetylation levels at replication forks using EdU in the SIRF assay. Acetylated H4K8 was detected at replication forks, which was increased upon replication stress generated by HU treatment (Figure 5C). Performing the same analysis in PCAF KO cells revealed a dependency of PCAF for H4K8Ac at replication forks, including upon HU treatment in either BRCA1- or BRCA2-deficient cells (Figures 5C and S7A). Similar results were obtained using iPOND followed by western blotting for H4K8ac at nascent DNA in control and HU treated conditions (Figure 5D). Input samples for our iPOND analysis revealed that bulk H4K8ac levels are not affected by PCAF loss, suggesting that other histone acetyltransferases can catalyze this histone modification in bulk chromatin. Thus, our results demonstrate that PCAF acetylates H4K8 specifically at replication forks. To investigate the function of PCAF-mediated H4K8ac in replication fork stability, we analyzed the requirement of MRE11- or EXO1-H4K8ac binding in replication fork degradation in BRCA2-deficient cells. For this analysis, we knocked down endogenous MRE11 or EXO1 using RNA interference to target their 3'UTRs, effects that were validated by western blotting and determined using DNA fiber assays to protect forks from degradation in BRCA2-depleted cells, as expected (Figures 5E–5H). While ectopic expression of MRE11 or EXO1 was able to complement these cells and promote fork degradation in these settings, expression of the H4K8ac binding mutants MRE11 1 or EXO1 PIN were not (Figures 5E–5H). In addition, these mutants displayed impaired binding to endogenous PCAF upon HU-treatment (Figures S7B and S7C). Taken together, these results demonstrate the importance of H4K8ac binding by MRE11 and EXO1 in fork degradation in BRCA2-deficient cells, suggesting that the association and activities of these nucleases at stalled forks require binding to the PCAF generated histone mark, H4K8ac.

Previous work revealed that H3K4me1/3 recruits MRE11 to replication forks (Ray Chaudhuri et al., 2016). To exclude the possibility that PCAF may regulate EXO1 and

MRE11 at the level of H3 methylation, we analyzed H3K4me1/3 levels using iPOND assay in WT and PCAF KO cells (Figure S7D). Consistent with our previous data, H4K8ac levels are decreased in PCAF KO cells while H3K4me1/3 levels are unaffected. Rescue of fork degradation can also proceed through the activities of replication fork remodelers, that act *via* their ability to reverse forks, which generate the substrates acted on by DNA nucleases (Bai et al., 2020; Kile et al., 2015; Kolinjivadi et al., 2017; Quinet et al., 2017b; Taglialatela et al., 2017; Vujanovic et al., 2017). To investigate PCAF and H4K8ac involvement in the regulation of fork remodelers, including SMARCAL1, ZRANB3 and HLTF, we compared the association of these factors to stalled forks in shCtrl and shPCAF HEK293 cells by iPOND (Figure S7E). Under these conditions, we observed the association of these fork remodelers with stalled forks in both WT and PCAF-depleted cells (Figure S7E). In addition, we did not observe any binding of these fork remodelers to H4K8ac (Figure S7F). While we cannot entirely rule out a connection between these other fork stability pathways and PCAF, our data suggests that PCAF regulation of replication fork stability acts primarily through the recruitment of MRE11/EXO1 to reversed forks by H4K8ac independently from the histone methylations H3K4me1/3 mediated by PTIP/MLL (Figure S7D) or EZH2 and H3K27me3 (Figure 3E) or fork remodelers (Figures S7E and S7F).

ATR phosphorylates PCAF serine 264 to prevent excessive replication fork degradation.

The ataxia telangiectasia and Rad3-related (ATR) kinase is a master regulator for genome stability during DNA replication. ATR phosphorylates various substrates to maintain genome integrity during DNA replication (Awasthi et al., 2015; Couch et al., 2013; Shiotani and Zou, 2009). For example, ATR suppresses SMARCAL1 DNA translocase activity *via* phosphorylation at serine 652 to prevent unregulated SMARCAL1-mediated fork reversal and collapse (Bansbach et al., 2009; Couch et al., 2013). *In silico* analysis revealed that PCAF has a conserved ATM/ATR phosphorylation consensus motif ($X(S*/T*)Q$) at its N-terminal domain, which is highly conserved in vertebrates (Figure 6A). Given our results identifying PCAF as a replication stress response factor, we tested if PCAF was also a target for ATR. To this end, endogenous and GFP-tagged PCAF was immunoprecipitated after HU-induced replication stress followed by western blotting with an anti-phospho(S/T)Q antibody (Figures 6B and 6C). Under these conditions, we observed PCAF phosphorylation specifically in HU-treated cells with CHK1 phosphorylation serving as a replication stress indicator. This signal was dependent on ATR, as treatment with the pharmacological ATR inhibitor (VE-821) reduced this signal as well as CHK1 phosphorylation, a known substrate of ATR (Figure 6B). In addition, an N-terminal domain deletion mutant of PCAF, which contains the ATR consensus motif, and PCAF S264A abolished the p(S/T)Q signal (Figures 6C and 6D). Taken together, our results reveal that ATR phosphorylates PCAF on serine 264 during DNA replication stress.

To investigate how ATR may regulate PCAF during these processes, we analyzed the interaction of PCAF phospho-mutant (S264A) with replication forks by iPOND. Interestingly, we observed that PCAF S264A (non-phosphorylatable mutant) displayed increased interactions with replication forks compared to WT (Figure 6E), suggesting that ATR phosphorylation may dampen the ability of PCAF to interact with replication forks. If this were the case, we would predict that ATR inhibition would promote H4K8ac, as well as

MRE11 and EXO1, accumulation at replication forks. To test this prediction, we performed iPOND in HU-treated cells in the presence of an ATR inhibitor. Interestingly, inhibition of ATR resulted in an increased association of WT PCAF with stalled replication forks (Figure 6F). As predicted, we also observed an increase of H4K8ac, as well as MRE11 and EXO1, at stalled replication forks in ATR-inhibited cells compared to untreated cells (Figure 6F).

ATR and its downstream effectors require replication fork dynamics upon replication stress, including fork reversal and degradation (Saldivar et al., 2017). Impaired ATR leads to the promotion of MRE11-mediated fork degradation, reactivation of PARPi sensitivity and irreversible DSBs (Brown and Baltimore, 2000; Couch et al., 2013; Toledo et al., 2013; Yazinski et al., 2017). Considering these previous works in light of our findings with PCAF, we predict that hyper-activated PCAF by ATR inhibition would result in MRE11/EXO1-mediated excessive fork degradation and DSBs. We sought to test this hypothesis by further investigating the relationship between ATR-mediated PCAF phosphorylation and replication fork degradation in BRCA2-deficient cells. As expected, ATR inhibition resulted in enhanced fork degradation in BRCA2-deficient U2OS WT cells (Figure 6G; (Saldivar et al., 2017)). Interestingly, enhanced fork degradation by ATR inhibition was dependent on PCAF since loss of PCAF rescued these effects (Figure 6G). The level of fork protection observed in PCAF KO cells depleted for BRCA2 was similar in untreated and ATRi-treated cells, suggesting that the ability of ATR to promote fork degradation in BRCA2-deficient cells is reliant on PCAF. Next, we measured DSB levels by neutral comet assay in PCAF KO cells. While PCAF KO cells reconstituted with PCAF WT did not display increased DSBs upon HU treatment unless ATR was inhibited, cells expressing the S264A phospho-dead PCAF mutant displayed induced DSBs under replication stress regardless of ATR inhibition (Figure 6H). Taken together, these observations indicate that ATR suppresses PCAF hyper-activation at stalled replication forks through phosphorylation on PCAF on S264, which prevents heightened replication stress and DSB formation.

DISCUSSION

This work identifies the histone acetyltransferase PCAF as a crucial replication fork stabilizer that functions through its chromatin modifying activity by acetylating H4K8 (Figure 7A). Recent studies have shown that the chromatin writers EZH2 and PTIPMLL3/4 catalyze H3K27me3 and H3K4me1/3 respectively at replication forks to recruit the nucleases MUS81 and MRE11 to induce fork degradation (Ray Chaudhuri et al., 2016; Rondinelli et al., 2017). These findings indicated that histone methylations play critical roles in replication fork stability and PARP inhibitor sensitivity. MUS81 interactions with H3K27me3 were mapped to a non-canonical methylation-binding region within a winged helix domain of MUS81 while MRE11 binding to methylated histone H3 remains unknown (Ray Chaudhuri et al., 2016; Rondinelli et al., 2017). Here, we identify histone acetylation by PCAF in promoting replication fork degradation in BRCA-deficient cells by promoting H4K8ac binding by MRE11 and EXO1 at replication forks (Figure 7A).

Mapped domains that mediate histone acetylation binding within MRE11 and EXO1 are unknown to harbor histone mark reader domains. It is of interest to note that the histone methylation binding domain of MUS81, as well as the regions we identify for histone

acetylation binding in MRE11 and EXO1 (Figures 4B–4E and S6) all map to regions reported to be involved in nucleic acid binding. Several defined chromatin reader domains, including PWWP, chromodomain and bromodomain have been shown to bind both histone modifications and nucleic acids (Miller et al., 2016; Morrison et al., 2017; Rona et al., 2016), suggesting that this may be a common feature of canonical and non-canonical chromatin reader domains. While searches with histone modification binding MRE11 and EXO1 motifs did not identify regions in other proteins that share homology, several additional DDR factors have DNA binding capabilities. Future studies are warranted to assess potential histone modification binding by these and other domains within chromatin and DNA-associated factors involved in genome integrity. Additional nucleases including DNA2/WRN helicase and FAN1 also promote replication fork degradation and fork restart (Porro et al., 2017; Thangavel et al., 2015). However, how these nucleases are recruited to damaged replication forks is unclear.

It is likely that multiple pathways are involved in regulating nucleases at stalled forks, as described here for MRE11, EXO1 and MUS81. In addition, we observed that PCAF-mediated replication processes appeared to operate independently of EZH2 and PTIP-MLL3/4 (Figures 3E and S7D). Loss of PCAF does not affect EZH2 accumulation at stalled replication forks and H3K4 methylation was unaffected by PCAF deficiency. Our results suggest that PCAF-mediated H4K8ac acts in a separate distinct pathway compared to the EZH2-H3K27me3-MUS81 axis or PTIP-MLL3/4-H3K4me1/3 that promotes MRE11 recruitment to stalled replication forks. Why both histone acetylation and methylation are required for MRE11 recruitment to stalled forks is unclear. MRE11 interacts directly with acetylated histones and may also bind methylated histones. These interactions may coordinate the levels of nucleases at stalled replication forks to prevent irregular DNA processing. MRE11 functions within a complex with RAD50 and NBS1 (Syed and Tainer, 2018), which may also interact with modified histones at stalled forks. In spite of these remaining questions, this work reveals the essential nature of histone modifying enzymes and histone post-translational modifications acting at replication forks to promote the association of nucleases with chromatin at stalled forks.

We demonstrate the molecular mechanisms that govern PCAF association with replication forks that mediate H4K8ac. PCAF utilizes its N-terminal domain for recruitment to stalled forks, as well as its acetylation activity towards H4K8 to facilitate MRE11 and EXO1 nuclease recruitment to replication forks. Unlike during DSB repair, the function of PCAF at stalled forks is not reliant on its bromodomain (Figures S5A and S5B), suggesting the importance of PCAF in fork stability is separate from its role in DSB repair (Kim et al., 2019b). PCAF can be found in the SAGA chromatin-remodeling complex, which recently has been shown to mediate an ubiquitin to acetylation switch on histone H2B K120 (Clouaire et al., 2018; Kim et al., 2019b). This pathway requires the HAT and BRD domains of PCAF. Given the involvement of this pathway in HR, we cannot rule out that H2B modifications and the SAGA complex may regulate additional processes at replication forks. These data reinforce the importance of PCAF in genome maintenance through both DSB repair and replication fork stability.

Given the potential for PCAF to promote fork degradation, a potentially dangerous process if left uncontrolled, we hypothesized the existence of mechanisms that would constrain these activities. Our data suggest the presence of at least two mechanisms that act to control PCAF activities at stalled replication forks. First, we identified PCAF as a phosphorylation target of ATR on serine 264 (Figures 6D and 7B). ATR signaling is known to orchestrate the spatiotemporal-regulation of replication forks through phosphorylation signaling that impacts the cell cycle checkpoints, origin firing and stabilization of replication forks (Saldivar et al., 2017; Toledo et al., 2013). For example, ATR phosphorylates SMARCAL1 on S562, which suppresses SMARCAL1 fork remodeling activity (Couch et al., 2013). In the absence of SMARCAL1 phosphorylation by ATR, reversed replication forks are generated and DSBs are formed (Fekairi et al., 2009). For PCAF, an inability to be phosphorylated by ATR results in increased accumulation of PCAF at replication forks. This causes unregulated MRE11 and EXO1 recruitment to stalled replication forks (Figure 6F), which induces excessive fork degradation and DSB formation (Figures 6G and 6H). Thus, our results reveal that ATR protects stalled replication forks by also phosphorylating PCAF, which limits its ability to modify chromatin and promote fork degradation at stalled replication forks. In addition, we observed low levels of PCAF in BRCA2-deficient tumors and cell lines. These observations point to another potential mechanism in BRCA2-deficient cells that would select for low levels of PCAF. We hypothesize that reduced PCAF levels may allow cells harboring *BRCA* mutations to survive the associated genome instability that is observed in *BRCA*-deficient tumors.

Our work has identified a previously unreported role for PCAF and histone acetylation in replication fork stability, demonstrating that PCAF impacts PARPi resistance in BRCA-deficient cells. Given that low levels of PCAF result in PARPi resistance in BRCA-deficient cancer cells, our results suggest that PCAF may be a useful biomarker for predicting PARPi responses in *BRCA2*-mutated cancers. PCAF inhibitors are being developed for examination in cancer treatment (Ahmad et al., 2012; Saadat and Gupta, 2012; Zhao et al., 2018), but our results suggest caution for applying this strategy in *BRCA*-deficient tumors. In addition, our findings may provide a molecular basis for the reported synergy observed between HDACi and PARPi treatments in *BRCA*-deficient cancers (Ha et al., 2014; Marijon et al., 2018; Rasmussen et al., 2016; Yin et al., 2018). Based on our findings, treatments that increase acetylation at replication forks (i.e. HDACi) will likely result in increased fork degradation and cell death. In summary, our data highlight the importance of chromatin modifiers in replication fork stability and chemotherapeutic responses in BRCA-deficient cells. This information may be leveraged to develop new therapies targeting epigenetic mechanisms in these cancers.

LIMITATIONS

Chromatin acts as a complex signaling platform, generating a series of localized modifications that orchestrate a biological process, including in cis at the replication fork. Other histone modifications, in addition to PCAF-mediated H4K8ac including H3K4me1/3 and H3K27me3, are also involved in fork degradation (Ray Chaudhuri et al., 2016; Rondinelli et al., 2017). Although these marks were not affected by PCAF loss, we cannot rule out that these modifications impact PCAF and that histone modifications collectively

regulate other fork stability pathways including fork remodelers (Quinet et al., 2017b). In addition to H4K8, sPCAF targets other histone and non-histone protein and is found associated with large protein complexes, including the SAGA complex (Cheon et al., 2020; Helmlinger and Tora, 2017; Kim et al., 2019b). Future studies are warranted to ascertain the contribution of other PCAF interacting proteins, regulators and acetylated targets in replication fork dynamics, which may also contribute to therapeutic responses in BRCA proficient and deficient cancer cells.

STAR★METHODS

RESOURCE AVAILABILITY

Lead Contact—Further information and requests for resources and reagents should be directed to and will be fulfilled by the Lead Contact, Kyle M. Miller (kyle.miller@austin.utexas.edu).

Materials Availability—The plasmids and cell lines generated for this study are available upon request.

Data and Code Availability—Original raw data have been deposited to Mendeley Data and are available at https://data.mendeley.com/datasets/35wphpgv48/draft?a=280018b1-e154-4d2fb054-e9b19fa00753.

EXPERIMENTAL MODEL AND SUBJECT DETAILS

Cell lines and cell culture—U2OS and HEK293 cells were purchased from ATCC and cultured in Dulbecco's modified Eagle's medium (DMEM) supplemented with 10% fetal bovine serum (FBS), 2 mM L-glutamine, 100 U/ml penicillin, and 100 μg/ml streptomycin. BRCA2 homozygous mutated (PEO1) and control (PEO4) human ovarian adenocarcinoma cancer cell lines were purchased from Sigma-Aldrich and were maintained in RPMI-1640 medium supplemented with 10% fetal bovine serum (FBS), 2 mM L-glutamine and 2 mM sodium pyruvate. Human breast cancer cells were grown in DMEM (MCF7, BT-20, MDA-MB-157, MDA-MB-231, Hs 578T, MDA-MB-436, MDA-MB-453, MDA-MB-468) or RPMI-1640 (T47-D, HCC38, HCC70, HCC1143, HCC1187, HCC1395, HCC1599, HCC1806, HCC1937, BT-474, BT-549, DU4475) supplemented with 10% fetal bovine serum (FBS), 2 mM L-glutamine, 100 U/ml penicillin, and 100 μg/ml streptomycin. HR reporter cells (U2OS based DR-GFP) and LacO-I-SceI-TetO cell line (U2OS based LacO×256) were kindly provided from Dr. Jeremy M. Stark (City of Hope, CA) and Dr. Tom Misteli (NIH), respectively. These cells were cultured in DMEM supplemented with 10% fetal bovine serum (FBS), 2 mM L-glutamine and 2 mM sodium pyruvate.

METHOD DETAILS

Cloning, plasmids and primers—PCAF was amplified by PCR from cDNA (U2OS cells) and cloned into pENTR/DTOPO (Invitrogen) vector. PCAF domains were identified using Uniprot-Prosite database. EGFP-MRE11 and -EXO1 were kindly provided by Dr. Tanya T. Paull (The University of Texas at Austin, TX). These clones were cloned into pENTR/DTOPO (Invitrogen) vector. ENTRY clones were transferred into DEST vector

(pcDNA6.2 N-EmGFP, pDEST-CMV-SFB and pDEST15-GST) using Gateway LR Cloning system (Invitrogen). All deletion mutants were generated by PCR and point-mutants were constructed using site-directed mutagenesis (Agilent Technologies), according to manufacturer's instructions. All mutants were validated by DNA sequencing and all primer sets used in this study are described in the Table S1.

Transfections—siRNA oligonucleotides were purchased from Sigma-Aldrich or Dharmacon. Sequence information of all siRNAs is summarized in the Table S2. PEO1 or PEO4 cells were transfected at 40% confluency with 100 nM of siRNA in 6-well plates using Lipofectamine RNAiMax (Invitrogen). The following day, cells were re-transfected with the same amount of siRNA after changing the media with growth medium. After 24 h, cells were trypsinized and re-plated into 6-well plates for clonogenic assay analysis, which were conducted 24 h after re-plating. For U2OS cells, 20 nM of siRNA was used to transfect cells that were plated at 60% confluency in 12-well plates using Lipofectamine RNAiMax (Invitrogen). Appropriate plasmid DNA (1 μg/12-well; 2 μg/6-well; 10 μg/10 cm; 30 μg/15 cm plate) were transfected with PEI reagent (Sigma-Aldrich) or Lipofectamine 2000 (Invitrogen), following manufacturer's protocols. Analyses of transfected cells were performed 48 h post-transfection.

Chemicals and Antibodies—Information for all chemicals and antibodies used in this study are summarized in the Key resource table. Treatment times and concentrations are described in each figure legend.

RT-qPCR for *PCAF* expression in Triple-Negative Breast Cancer cells—A Triple-Negative Breast Cancer Panel (ATCC, #TCP-1003™) containing 17 different cell lines (BT-20, BT-549, MDA-MB-157, MDA-MB-231, Hs 578T, MDA-MB-436, MDA-MB-453, MDA-MB-468, HCC38, HCC70, HCC1143, HCC1187, HCC1395, HCC1599, HCC1806, HCC1937, DU4475) encompassing all six Triple Negative Breast Cancer (TNBC) subtypes (Lehmann et al., 2011) was obtained from ATCC. Cells were seeded at 10^5 cells/mL in a 3 cm diameter dish, and were lysed 48 h later in 300 μL of SKP buffer (RNA/Protein Purification Plus kit; Norgen, #48200) supplemented with 10 μL of beta-mercaptoethanol per mL of SKP buffer and frozen at −80 °C. The frozen lysates were thawed, and RNA and protein was purified using the RNA/Protein purification Plus kit (Norgen, #48200) according to the manufacturer's recommendation. 250 ng of total RNA was reverse transcribed into cDNA with the qScript cDNA SuperMix kit (Quantabio, #95048). Subsequently, 1/20th of each reaction was used for real-time PCR on a StepOne Plus system with gene specific primers. qPCR primer sequences are described in the Table S1.

Western blotting—Samples were separated on an 8–16% gradient SDS-PAGE gel for 1.5 h (120 V) and transferred onto nitrocellulose membrane (GE Healthcare, #10600007) for 2 h (100 V). Transferred membranes were blocked with 5% BSA in TBS-T (0.05% Tween-20) for 1 h and then incubated with the specific primary antibody (diluted in 3% BSA (TBS-T)) for 18 h at 4°C with gentle shaking. Membranes were washed 3 times (10 min) with TBS-T and incubated with the appropriate secondary antibody (diluted in 3% BSA (TBS-T)) for 1 h

at RT, with gentle shaking. After incubation, membranes were again washed three times (10 min) in TBS-T and detected using ECL (GE Healthcare, #RPN2232). Membranes were imaged with a ChemiDoc (Bio-rad) instrument by chemiluminescence.

Generation of PCAF knockout (KO) or knockdown (KD) cell lines—PCAF knockout (KO) cells were generated as described previously (Kim et al., 2019b). Briefly, PCAF targeting gRNAs were cloned into the pSpCas9 (BB)-2A-Puro (PX459, Addgene #48139) vector and transfected using Lipofectamine 2000 (Invitrogen) in U2OS cells. After 48 h, transfected cells were selected in puromycin (500 ng/ml) containing medium for 3–5 days and re-plated in 96-well plates by limited dilution to obtain single cell clones. For generation of PCAF knockdown (KD) HEK293 cell lines, shRNA against PCAF in pLKO.1 lentiviral backbone was obtained from Sigma-Aldrich (#TRCN0000018528). pMD2.G (envelope plasmid) and psPAX2 (packaging plasmid) were co-transfected with pLKO.1 shRNA (non-target shCtrl or shPCAF) using Lipofectamine 2000 (Invitrogen) into HEK293 cells to generate lentivirus. On the following day, transfected cells were changed with fresh medium and then, lentivirus containing medium was harvested after 48 h, 72 h post-transfection. For viral transduction, HEK293 cells were seeded at 10^5 cells/mL in 6 cm diameter dish and infected after 24 h with 1.5 ml of virus containing medium in the presence of polybrene (8.3 μg/ml). The next day, infected cells were selected in puromycin (2 μg/ml) containing growth medium. Endogenous PCAF protein levels were confirmed by western blotting with anti-PCAF antibody to validate knockout and knockdown efficiencies (Cell Signaling, #3378).

Clonogenic cell survival assay—U2OS cells were transfected with indicated siRNAs and incubated for 24 h. Cells were re-seeded into 6-well plates and on the following day, cells were continuously treated with PARP inhibitor (0–2 μM Olaparib) for 14 days in a tissue culture incubator (37°C, 5% CO_2). PEO1 and PEO4 cells were transfected two times with indicated siRNAs and re-plated into 6-well plates. After 24 h, cells were treated with PARP inhibitor (0–4 μM Olaparib) for 3 days and washed with fresh growth medium. Cells were then incubated in a tissue culture incubator for 14 days. Colonies were fixed with 100% (v/v) methanol for 10 min and fixed colonies were stained with crystal violet solution (0.5% crystal violet in 20% ethanol) for 20 min. Plates were washed with water and the stained colonies were counted and normalized to plating efficiencies of untreated cells for each siRNA.

HR repair assay—HR repair assay was performed as previously described (Gong et al., 2015; Gunn et al., 2011). Briefly, U2OS-based HR reporter cells (U2OS-DR-GFP) were transfected with indicated siRNAs by Lipofectamine RNAiMax (Invitrogen). On the following day, pCAG-I-SceI was transfected into HR reporter cells and incubated for 48 h. After incubation, cells were harvested and washed with 1 ml of PBS. Pellets were resuspended in 500 μl of PBS and repair efficiency was analyzed as the percentage of GFP-positive cells by a flow cytometer (BD Accuri™ C6). Results were normalized to values obtained for siControl (siCtrl) transfected cells and results were graphed using Prism software (GraphPad).

Immunofluorescence of DDR factors—U2OS cells were transfected with indicated siRNAs and incubated for 48 h. Cells were then treated with IR (5 Gy) and immunofluorescence (IF) analysis was performed after 2 h further incubation in tissue culture incubator (37°C, 5% CO_2). Cells were pre-extracted with 1 ml of CSK buffer containing 10 mM PIPES, pH 6.8, 100 mM NaCl, 300 mM sucrose, 3 mM $MgCl_2$, 1 mM EGTA and 0.5% (v/v) Triton X-100 on ice for 5 min followed by fixation with 2% paraformaldehyde (PFA) for 15 min at RT. Subsequently, cells were washed 3 times with PBS (1 ml) and blocked with 1 ml of 3% BSA in TBS-T (0.05% Tween-20) for 30 min. RAD51 antibody (GeneTex, #GTX100469) was incubated for 18 h at 4°C and then washed with 1 ml of PBS (10 min, 3 times) at RT. After washing, cells were incubated with Alexa Fluor 594 goat anti-rabbit IgG (Invitrogen, #A-11012) for 1 h at RT and mounted onto 1.2 mm glass slide using DAPI containing Vectashield mounting medium (Vector laboratories, #H-1200). Samples were analyzed using a Fluoview 3000 confocal microscope (Olympus) and the number of RAD51 foci per cell was counted.

LacO array system—LacO array system was performed as previously described (Beuzer et al., 2014; Burgess et al., 2014; Kim et al., 2018). Briefly, a LacO-I-SceI-TetO cell line (LacO×256) was transfected either alone with mCherry-tagged LacR or also with GFP-tagged proteins as indicated. After 48 h, cells were incubated with 10 μM EdU for S phase discrimination, and fixed with 2% PFA for 15 min at RT. Incorporated EdU was Click-labeled using azide-linked Alexa Fluor 647 (Invitrogen), following manufacturer's instructions.

EdU incorporation assay for imaging—To measure replicating cells, the incorporation of EdU (5-ethynyl-2'-deoxyuridine) into DNA during DNA synthesis was detected using Click-iT EdU Imaging Kit (Invitrogen). In brief, pre-warmed 2x EdU solution was added into media containing cells at 1x to give a final concentration of 10 μM for 30 min. Cells were fixed with 2% PFA for 15 min and detected by Click-iT reaction according to the manufacturer's instructions. Subsequently, cells were stained with primary (18 h incubation at 4°C) and secondary (1 h incubation at RT) antibodies as indicated and analyzed by a Fluoview 3000 confocal microscope (Olympus).

SIRF assay—The SIRF assay (*in situ* protein interactions at nascent and stalled replication forks) was performed as described previously with minor modification to detect replication fork interacting proteins and histone modifications (Roy et al., 2018). In brief, U2OS cells were incubated with 125 μM EdU for 8 min and treated with 4 mM HU for 3 h after PBS washing (2 times). After treatment, cells were fixed with 2% PFA for 15 min at RT and permeabilized with 0.25% Triton X-100 for 15 min. Cells were washed 3 times for 5 min with PBS and the Click-iT reaction was performed for 1 h at RT. Subsequently, cells were washed 2 times with PBS for 5 min, and blocked with blocking buffer (10% goat serum and 0.1% Triton X-100) for 1 h at RT. Primary antibodies were diluted in the blocking buffer and incubated overnight at 4°C. Cells were then washed 3 times for 10 min with 1 ml of washing buffer A (0.01 M Tris, pH7.4, 0.15 M NaCl, and 0.05% Tween-20) for 5 min each. In the meantime, Duolink *In Situ* PLA probes (Sigma-Aldrich) anti-mouse (+) and anti-rabbit (−) were diluted (1:5) in blocking buffer. After washing, cells were incubated with diluted PLA

probes for 1 h at 37°C and again washed in 1 ml of washing buffer A (3 times, 10 min). Next, cells were incubated with the ligation mix for 30 min at 37°C and washed (3 times, 10 min) in 1 ml of washing buffer A. Finally, the cells were incubated with the amplification mix for 100 min at 37°C and washed (3 times, 5 min) with washing buffer B (0.2 M Tris and 0.1 M NaCl). Finally, cells were mounted with DAPI containing Vectashield mounting medium (Vector laboratories, #H-1200) and detected using a Fluoview 3000 confocal microscope (Olympus). For each SIRF assay, at least 100 cells were analyzed and quantified by ImageJ (NIH).

DNA fiber assay—DNA fiber assay was performed as described previously with minor modifications (Merrick et al., 2004; Mukherjee et al., 2019; Quinet et al., 2017a; Ray Chaudhuri et al., 2016). Briefly, cells were treated with CIdU (30 μM), IdU (250 μM) and HU (4 mM), with PBS wash (3 times) between each treatment (treatment order and times are indicated in each figure). After the treatments, cells were washed with 1 ml of PBS and trypsinized for 2 min. Cells were harvested with 1 ml of normal growth medium (DMEM supplemented with 10% FBS, 2 mM L-glutamine, 100 U/ml penicillin, and 100 μg/ml streptomycin) and centrifuged for 3 min at 1,500 rpm. Pellets were resuspended in 100 μl of PBS and 2 μl of cells containing PBS were gently mixed with 8 μl of lysis buffer (200 mM Tris, pH 7.4, 50 mM EDTA, 0.5% SDS). Cells were lysed for 8 min at RT and lysed cells were dropped on a manually tilted glass slide (30°–45°) to allow the cell suspension to run slowly down the slide. Slides containing fibers were air-dried and fixed with methanol/acetic acid (3:1) for 10 min at RT. DNA fibers on slides were denatured with 2.5 M HCl for 1 h, washed 3 times with PBS for 5 min, and blocked with blocking solution (2% BSA, 0.1% Tween 20, 1x PBS; 0.22 μm filtered) for 30 min. The newly replicating CIdU and IdU tracts were stained with anti-BrdU antibodies (Abcam, #ab6326 and BD Biosciences, #347580) and DNA fibers were visualized by Fluoview 3000 confocal microscope (Olympus). IdU/CIdU ratios were measured using ImageJ (NIH) and graphs were generated using Prism software (GraphPad).

iPOND—iPOND was performed as described (Dungrawala and Cortez, 2015; Leung et al., 2013; Rondinelli et al., 2017). Briefly, cells (ten 15 cm dishes) were pulsed with 10 μM EdU for 15 min then treated with 10 μM thymidine (2 h) or 4 mM hydroxyurea (2 h). After treatment, cells were cross-linked with 1% formaldehyde for 10 min and quenched with 125 mM glycine for 5 min at RT. Cells were washed 3 times with PBS and permeabilized with 0.25% Triton X-100 in PBS for 30 min at 4°C. Then, cells were washed once with PBS and subjected to the Click-iT reaction for 1 h at 4°C with gentle rotation. Cells were centrifuged at 2,500 g for 10 min (4°C) and washed 2 times with PBS. The pellet was then lysed with 500 μl of lysis buffer (50 mM Tris-HCl pH 8.0, 1% SDS, and 1x protease inhibitors), followed by sonication (three 10s ON / 10s OFF cycles). Samples were centrifuged at 15,000 rpm for 10 min at 4°C and the supernatant was IPed with streptavidin-beads overnight at 4°C. Beads were washed 3 times for 10 min with 1 ml of lysis buffer and boiled with SDS sample buffer for 30 min. Boiled samples were centrifuged for 10 min at 15,000 rpm and supernatants were separated on an 8–16% gradient gel and analyzed by western blotting.

Histone binding and peptide pull-down assay—These experiments were performed as previously described (Gong et al., 2015; Kim et al., 2019b). For modified histone binding assays, a histone peptide array (Active Motif) was blocked with 5% BSA in TBS-T at RT for 1 h and incubated with full-length human MRE11/RAD50 or EXO1 recombinant proteins (purified from insect cells; (Yang et al., 2013)) for 2 h at 4°C. After incubating with recombinant proteins, the histone peptide array was washed three times (5 min) with TBS-T followed by incubation with primary antibody at 4°C for 18 h. The next day, the array was washed (3 times, 5 min) with TBS-T and incubated with secondary HRP-conjugated antibody for 1 h at RT. After incubation, the histone peptide array was washed 3 times for 10 min with TBS-T and detected using ECL (GE Healthcare, #RPN2232). Array was imaged with a ChemiDoc (Bio-rad) instrument and the binding intensity was calculated by Array analyze software from MODified™ Histone peptide array (Active Motif). To validate the histone peptide array results, peptide pull-down assays were performed using recombinant proteins or cells lysates from HEK293 cells. Streptavidin T1 Dynabeads (Invitrogen, #65601) were pre-incubated with biotinylated histone peptides at 4°C for 1 h and unbound peptides were removed by bead washing (3 times) with NETN buffer (10 mM Tris, pH 8.0, 150 mM NaCl, 0.5% NP-40, supplemented with 1x protease inhibitor cocktail from Roche). During incubation of the peptides with beads, HEK293 cells were lysed with 120 U/ml TurboNuclease (Accelagen) containing NETN buffer and lysates were centrifuged at 15,000 rpm at 4°C for 10 min. Resulting supernatants were incubated with peptide-bound beads at 4°C for 18 h. Samples were washed 3 times for 10 min at 4°C with lysis buffer and bound proteins were eluted using 2x SDS sample buffer for 5 min at 95°C. Boiled samples were centrifuged for 10 min at 15,000 rpm and the supernatants were analyzed by western blot.

Immunoprecipitation—Immunoprecipitation analysis was performed to analyze protein interactions. Cells (10 cm dish) were lysed using 1 mL of NETN buffer (10 mM Tris, pH 8.0, 150 mM NaCl, 0.5% NP-40, supplemented with 1x protease inhibitor cocktail from Roche and 1x phosphatase inhibitor cocktail from Thermo Scientific) for 1 h at 4°C. Samples were collected and centrifuged at 15,000 rpm for 10 min at 4°C. Supernatants were taken and incubated with 1 μg of the indicated primary antibody overnight at 4°C while rotating. The following day, samples were re-incubated with 10 μl of protein A/G beads (Thermo Scientific) for 4 h at 4°C. After incubation, beads were washed 3 times for 10 min at 4°C with NETN buffer, and bound proteins were eluted from beads with 2x SDS sample buffer. Samples were boiled for 5 min at 98°C and separated by an 8–16% gradient SDS-PAGE gel, followed by western blot analysis. For GFP-tagged proteins, lysed supernatants were incubated with 15 μl GFP-Trap magnetic beads (ChromoTek) for 18 h at 4°C. Beads were washed 3 times for 10 min at 4°C with NETN buffer, and boiled with 2x SDS sample buffer. Samples were centrifuged for 10 min at 15,000 rpm and supernatant were subjected to western blot analysis as described above.

Laser micro-irradiation and live-cell imaging—Laser micro-irradiation and live-cell imaging methods were performed as described (Kim et al., 2019a). Briefly, cells were seeded on glass-bottomed dishes (Ted Pella) and pre-sensitized with 10 μM BrdU for 24 h before laser-induced damage. Cells were visualized with 60X oil objective lens and laser-induced DNA damages were generated by a 405-nm laser beam (60% laser intensity) using a

Fluoview 3000 confocal microscope (Olympus). During laser damage and live-cell imaging, cells were maintained in an environmental chamber (37°C, 5% CO_2). All experiments were analyzed using FV-10-ASW3.1 software (Olympus). Fluorescence intensity at damage sites was calculated by comparing the intensity of damaged versus non-damaged sites within the same cell as a function of time. For each group, at least 10 individual cells were analyzed and quantification results were graphed using Prism software (GraphPad).

Neutral comet assay—Neutral comet assay was performed to measure DSBs using CometAssay Reagent Kit (Trevigen) in accordance with the manufacturer's instructions. GFP-PCAF WT and S264A (phospho-dead mutant) were transfected with siRNAs targeting BRCA2 in PCAF KO cells. Cells were incubated for 48 h and co-treated with HU (4 mM) and ATR inhibitor (5 μM). After 2 h further incubation, cells were washed once with PBS and trypsinized by incubation with trypsin-EDTA for 2 min. Cells were collected with normal growth medium and centrifuged for 3 min at 1,500 rpm. The pellet was mixed with LMAgarose (Trevigen) and samples were placed on glass slides and cells were lysed with lysis solution (100 μl, Trevigen) for 1 h at 4°C. Slides containing lysed cells were placed in a submerged horizontal electrophoresis apparatus (Bio-rad) and electrophoresed (1 V/cm^2) for 40 min in TBE buffer. Samples were fixed with 70% EtOH for 10 min and dried for 18 h at RT. On the following day, slides were stained with SYBR-green (Invitrogen) for 3 min and images of stained DNA was obtained using a Fluoview 3000 confocal microscope (Olympus). Comet tail moments were calculated using ImageJ (v 1.48) and analyzed by Prism software (GraphPad). Tail moment (TM) reflects both the tail length (TL) and the fraction of DNA in the comet tail (TM = %DNA in tail $\times$ TL/100).

Bioinformatic analysis of public patient data—Publicly available mRNA expression (Z-score) and somatic mutation profiles of breast cancer were obtained from cBioPortal (TCGA, (Cancer Genome Atlas, 2012), http://cbioportal.org/). After matching sample labels on each platform, the data sets (n=481) were used for the analysis. To verify the prognosis according to PCAF expression by BRCA1/2 mutation status in ovarian cancers, we obtained multilayered profiles for mRNA expression (FPKM) and somatic mutation profiles of ovarian cancer (OV) from TCGA data portal (https://portal.gdc.cancer.gov). Gene expression profile was normalized by log2 transformation, aggregated by HUGO official symbol, and centered by subtracting the median values for each sample. After matching sample labels on each platform, the data sets (n=274) were used for Kaplan-Meier analysis. We divided the TCGA-OC patients into three cohorts according to BRCA1/2 mutation status: BRCA1/2-wild-type (n=231), BRCA1-mutated (n=20) and BRCA2-mutated (n=32). Each cohort was divided into two groups by Q80 of the expression levels of *PCAF* gene, and their prognostic significance for overall survival was estimated based on the Cox proportional hazards regression model using the 'survival' R package.

Quantification and statistical analysis—Statistical calculations were done using Prism (GraphPad). Two-tailed Student's *t*-test, one-way analysis of variance (Ogryzko et al.) by a Dunnett multiple comparison test and Mann-Whitney test were used to determine statistical significance as indicated for all datasets in each figure legend. All experiments

were performed at least twice unless otherwise indicated, and *P*-values and sample sizes are indicated in the figures and/or figure legends.

Supplementary Material

Refer to Web version on PubMed Central for supplementary material.

ACKNOWLEDGMENTS

REFERENCES

Ahmad A, Sarkar SH, Aboukameel A, Ali S, Biersack B, Seibt S, Li Y, Bao B, Kong D, Banerjee S, et al. (2012). Anticancer action of garcinol in vitro and in vivo is in part mediated through inhibition of STAT-3 signaling. Carcinogenesis 33, 2450–2456. [PubMed: 22971573]

Arcus VL, McKenzie JL, Robson J, and Cook GM (2011). The PIN-domain ribonucleases and the prokaryotic VapBC toxin-antitoxin array. Protein Eng Des Sel 24, 33–40. [PubMed: 21036780]

Awasthi P, Foiani M, and Kumar A (2015). ATM and ATR signaling at a glance. J Cell Sci 128, 4255–4262. [PubMed: 26567218]

Bai G, Kermi C, Stoy H, Schiltz CJ, Bacal J, Zaino AM, Hadden MK, Eichman BF, Lopes M, and Cimprich KA (2020). HLTF Promotes Fork Reversal, Limiting Replication Stress Resistance and Preventing Multiple Mechanisms of Unrestrained DNA Synthesis. Mol Cell 78, 1237–1251 e1237. [PubMed: 32442397]

Bansbach CE, Betous R, Lovejoy CA, Glick GG, and Cortez D (2009). The annealing helicase SMARCAL1 maintains genome integrity at stalled replication forks. Genes Dev 23, 2405–2414. [PubMed: 19793861]

Bast RC Jr., Hennessy B, and Mills GB (2009). The biology of ovarian cancer: new opportunities for translation. Nat Rev Cancer 9, 415–428. [PubMed: 19461667]

Beuzer P, Quivy JP, and Almouzni G (2014). Establishment of a replication fork barrier following induction of DNA binding in mammalian cells. Cell Cycle 13, 1607–1616. [PubMed: 24675882]

Bouwman P, Aly A, Escandell JM, Pieterse M, Bartkova J, van der Gulden H, Hiddingh S, Thanasoula M, Kulkarni A, Yang Q, et al. (2010). 53BP1 loss rescues BRCA1 deficiency and is associated with triple-negative and BRCA-mutated breast cancers. Nat Struct Mol Biol 17, 688–695. [PubMed: 20453858]

Brown EJ, and Baltimore D (2000). ATR disruption leads to chromosomal fragmentation and early embryonic lethality. Genes Dev 14, 397–402. [PubMed: 10691732]

Bryant HE, Schultz N, Thomas HD, Parker KM, Flower D, Lopez E, Kyle S, Meuth M, Curtin NJ, and Helleday T (2005). Specific killing of BRCA2-deficient tumours with inhibitors of poly(ADP-ribose) polymerase. Nature 434, 913–917. [PubMed: 15829966]

Burgess RC, Burman B, Kruhlak MJ, and Misteli T (2014). Activation of DNA damage response signaling by condensed chromatin. Cell Rep 9, 1703–1717. [PubMed: 25464843]

Cancer Genome Atlas N (2012). Comprehensive molecular portraits of human breast tumours. Nature 490, 61–70. [PubMed: 23000897]

Cheon Y, Kim H, Park K, Kim M, and Lee D (2020). Dynamic modules of the coactivator SAGA in eukaryotic transcription. Exp Mol Med.

Chiu LY, Gong F, and Miller KM (2017). Bromodomain proteins: repairing DNA damage within chromatin. Philos Trans R Soc Lond B Biol Sci 372.

Clements A, Rojas JR, Trievel RC, Wang L, Berger SL, and Marmorstein R (1999). Crystal structure of the histone acetyltransferase domain of the human PCAF transcriptional regulator bound to coenzyme A. EMBO J 18, 3521–3532. [PubMed: 10393169]

Clouaire T, Rocher V, Lashgari A, Arnould C, Aguirrebengoa M, Biernacka A, Skrzypczak M, Aymard F, Fongang B, Dojer N, et al. (2018). Comprehensive Mapping of Histone Modifications at DNA Double-Strand Breaks Deciphers Repair Pathway Chromatin Signatures. Mol Cell 72, 250–262 e256. [PubMed: 30270107]

Couch FB, Bansbach CE, Driscoll R, Luzwick JW, Glick GG, Betous R, Carroll CM, Jung SY, Qin J, Cimprich KA, et al. (2013). ATR phosphorylates SMARCAL1 to prevent replication fork collapse. Genes Dev 27, 1610–1623. [PubMed: 23873943]

Couch FJ, Nathanson KL, and Offit K (2014). Two decades after BRCA: setting paradigms in personalized cancer care and prevention. Science 343, 1466–1470. [PubMed: 24675953]

Dhalluin C, Carlson JE, Zeng L, He C, Aggarwal AK, and Zhou MM (1999). Structure and ligand of a histone acetyltransferase bromodomain. Nature 399, 491–496. [PubMed: 10365964]

Dungrawala H, and Cortez D (2015). Purification of proteins on newly synthesized DNA using iPOND. Methods Mol Biol 1228, 123–131. [PubMed: 25311126]

Farmer H, McCabe N, Lord CJ, Tutt AN, Johnson DA, Richardson TB, Santarosa M, Dillon KJ, Hickson I, Knights C, et al. (2005). Targeting the DNA repair defect in BRCA mutant cells as a therapeutic strategy. Nature 434, 917–921. [PubMed: 15829967]

Fekairi S, Scaglione S, Chahwan C, Taylor ER, Tissier A, Coulon S, Dong MQ, Ruse C, Yates JR 3rd, Russell P, et al. (2009). Human SLX4 is a Holliday junction resolvase subunit that binds multiple DNA repair/recombination endonucleases. Cell 138, 78–89. [PubMed: 19596236]

Filippakopoulos P, Picaud S, Mangos M, Keates T, Lambert JP, Barsyte-Lovejoy D, Felletar I, Volkmer R, Muller S, Pawson T, et al. (2012). Histone recognition and large-scale structural analysis of the human bromodomain family. Cell 149, 214–231. [PubMed: 22464331]

Fujisawa T, and Filippakopoulos P (2017). Functions of bromodomain-containing proteins and their roles in homeostasis and cancer. Nat Rev Mol Cell Biol 18, 246–262. [PubMed: 28053347]

Glavan F, Behm-Ansmant I, Izaurralde E, and Conti E (2006). Structures of the PIN domains of SMG6 and SMG5 reveal a nuclease within the mRNA surveillance complex. EMBO J 25, 5117–5125. [PubMed: 17053788]

Gong F, Chiu LY, Cox B, Aymard F, Clouaire T, Leung JW, Cammarata M, Perez M, Agarwal P, Brodbelt JS, et al. (2015). Screen identifies bromodomain protein ZMYND8 in chromatin recognition of transcription-associated DNA damage that promotes homologous recombination. Genes Dev 29, 197–211. [PubMed: 25593309]

Gong F, Chiu LY, and Miller KM (2016). Acetylation Reader Proteins: Linking Acetylation Signaling to Genome Maintenance and Cancer. PLoS Genet 12, e1006272. [PubMed: 27631103]

Gudmundsdottir K, and Ashworth A (2006). The roles of BRCA1 and BRCA2 and associated proteins in the maintenance of genomic stability. Oncogene 25, 5864–5874. [PubMed: 16998501]

Guillemette S, Serra RW, Peng M, Hayes JA, Konstantinopoulos PA, Green MR, and Cantor SB (2015). Resistance to therapy in BRCA2 mutant cells due to loss of the nucleosome remodeling factor CHD4. Genes Dev 29, 489–494. [PubMed: 25737278]

Gunn A, Bennardo N, Cheng A, and Stark JM (2011). Correct end use during end joining of multiple chromosomal double strand breaks is influenced by repair protein RAD50, DNA-dependent protein kinase DNA-PKcs, and transcription context. J Biol Chem 286, 42470–42482. [PubMed: 22027841]

Ha K, Fiskus W, Choi DS, Bhaskara S, Cerchietti L, Devaraj SG, Shah B, Sharma S, Chang JC, Melnick AM, et al. (2014). Histone deacetylase inhibitor treatment induces 'BRCAness' and synergistic lethality with PARP inhibitor and cisplatin against human triple negative breast cancer cells. Oncotarget 5, 5637–5650. [PubMed: 25026298]

Hanahan D, and Weinberg RA (2011). Hallmarks of cancer: the next generation. Cell 144, 646–674. [PubMed: 21376230]

He H, Wang J, and Liu T (2017). UV-Induced RPA1 Acetylation Promotes Nucleotide Excision Repair. Cell Rep 20, 2010–2025. [PubMed: 28854355]

Helmlinger D, and Tora L (2017). Sharing the SAGA. Trends Biochem Sci 42, 850–861. [PubMed: 28964624]

Higgs MR, Sato K, Reynolds JJ, Begum S, Bayley R, Goula A, Vernet A, Paquin KL, Skalnik DG, Kobayashi W, et al. (2018). Histone Methylation by SETD1A Protects Nascent DNA through the Nucleosome Chaperone Activity of FANCD2. Mol Cell 71, 25–41 e26. [PubMed: 29937342]

Hopkins TA, Shi Y, Rodriguez LE, Solomon LR, Donawho CK, DiGiammarino EL, Panchal SC, Wilsbacher JL, Gao W, Olson AM, et al. (2015). Mechanistic Dissection of PARP1 Trapping and the Impact on In Vivo Tolerability and Efficacy of PARP Inhibitors. Mol Cancer Res 13, 1465–1477. [PubMed: 26217019]

Jaspers JE, Kersbergen A, Boon U, Sol W, van Deemter L, Zander SA, Drost R, Wientjens E, Ji J, Aly A, et al. (2013). Loss of 53BP1 causes PARP inhibitor resistance in Brca1-mutated mouse mammary tumors. Cancer Discov 3, 68–81. [PubMed: 23103855]

Kennedy RD, and D'Andrea AD (2006). DNA repair pathways in clinical practice: lessons from pediatric cancer susceptibility syndromes. J Clin Oncol 24, 3799–3808. [PubMed: 16896009]

Kile AC, Chavez DA, Bacal J, Eldirany S, Korzhnev DM, Bezsonova I, Eichman BF, and Cimprich KA (2015). HLTF's Ancient HIRAN Domain Binds 3' DNA Ends to Drive Replication Fork Reversal. Mol Cell 58, 1090–1100. [PubMed: 26051180]

Kim J, Sturgill D, Sebastian R, Khurana S, Tran AD, Edwards GB, Kruswick A, Burkett S, Hosogane EK, Hannon WW, et al. (2018). Replication Stress Shapes a Protective Chromatin Environment across Fragile Genomic Regions. Mol Cell 69, 36–47 e37. [PubMed: 29249653]

Kim JJ, Kumbhar R, Gong F, and Miller KM (2019a). In Time and Space: Laser Microirradiation and the DNA Damage Response. Methods Mol Biol 1999, 61–74. [PubMed: 31127569]

Kim JJ, Lee SY, Gong F, Battenhouse AM, Boutz DR, Bashyal A, Refvik ST, Chiang CM, Xhemalce B, Paull TT, et al. (2019b). Systematic bromodomain protein screens identify homologous recombination and R-loop suppression pathways involved in genome integrity. Genes Dev 33, 1751–1774. [PubMed: 31753913]

Kim JJ, Lee SY, and Miller KM (2019c). Preserving genome integrity and function: the DNA damage response and histone modifications. Crit Rev Biochem Mol Biol 54, 208–241. [PubMed: 31164001]

King MC (2014). "The race" to clone BRCA1. Science 343, 1462–1465. [PubMed: 24675952]

Kolinjivadi AM, Sannino V, De Antoni A, Zadorozhny K, Kilkenny M, Techer H, Baldi G, Shen R, Ciccia A, Pellegrini L, et al. (2017). Smarcal1-Mediated Fork Reversal Triggers Mre11-Dependent Degradation of Nascent DNA in the Absence of Brca2 and Stable Rad51 Nucleofilaments. Mol Cell 67, 867–881 e867. [PubMed: 28757209]

Lehmann BD, Bauer JA, Chen X, Sanders ME, Chakravarthy AB, Shyr Y, and Pietenpol JA (2011). Identification of human triple-negative breast cancer subtypes and preclinical models for selection of targeted therapies. J Clin Invest 121, 2750–2767. [PubMed: 21633166]

Lemacon D, Jackson J, Quinet A, Brickner JR, Li S, Yazinski S, You Z, Ira G, Zou L, Mosammaparast N, et al. (2017). MRE11 and EXO1 nucleases degrade reversed forks and elicit MUS81-dependent fork rescue in BRCA2-deficient cells. Nat Commun 8, 860. [PubMed: 29038425]

Leung KH, Abou El Hassan M, and Bremner R (2013). A rapid and efficient method to purify proteins at replication forks under native conditions. Biotechniques 55, 204–206. [PubMed: 24107252]

Li Y, Li Z, Dong L, Tang M, Zhang P, Zhang C, Cao Z, Zhu Q, Chen Y, Wang H, et al. (2018). Histone H1 acetylation at lysine 85 regulates chromatin condensation and genome stability upon DNA damage. Nucleic Acids Res 46, 7716–7730. [PubMed: 29982688]

Liao H, Ji F, Helleday T, and Ying S (2018). Mechanisms for stalled replication fork stabilization: new targets for synthetic lethality strategies in cancer treatments. EMBO Rep 19.

Lord CJ, and Ashworth A (2012). The DNA damage response and cancer therapy. Nature 481, 287–294. [PubMed: 22258607]

MacAlpine DM, and Almouzni G (2013). Chromatin and DNA replication. Cold Spring Harb Perspect Biol 5, a010207. [PubMed: 23751185]

Marijon H, Lee DH, Ding L, Sun H, Gery S, de Gramont A, and Koeffler HP (2018). Co-targeting poly(ADP-ribose) polymerase (PARP) and histone deacetylase (HDAC) in triple-negative breast cancer: Higher synergism in BRCA mutated cells. Biomed Pharmacother 99, 543–551. [PubMed: 29902865]

Merrick CJ, Jackson D, and Diffley JF (2004). Visualization of altered replication dynamics after DNA damage in human cells. J Biol Chem 279, 20067–20075. [PubMed: 14982920]

Mijic S, Zellweger R, Chappidi N, Berti M, Jacobs K, Mutreja K, Ursich S, Ray Chaudhuri A, Nussenzweig A, Janscak P, et al. (2017). Replication fork reversal triggers fork degradation in BRCA2-defective cells. Nat Commun 8, 859. [PubMed: 29038466]

Miller TC, Simon B, Rybin V, Grotsch H, Curtet S, Khochbin S, Carlomagno T, and Muller CW (2016). A bromodomain-DNA interaction facilitates acetylation-dependent bivalent nucleosome recognition by the BET protein BRDT. Nat Commun 7, 13855. [PubMed: 27991587]

Morrison EA, Sanchez JC, Ronan JL, Farrell DP, Varzavand K, Johnson JK, Gu BX, Crabtree GR, and Musselman CA (2017). DNA binding drives the association of BRG1/hBRM bromodomains with nucleosomes. Nat Commun 8, 16080. [PubMed: 28706277]

Mukherjee C, Tripathi V, Manolika EM, Heijink AM, Ricci G, Merzouk S, de Boer HR, Demmers J, van Vugt M, and Ray Chaudhuri A (2019). RIF1 promotes replication fork protection and efficient restart to maintain genome stability. Nat Commun 10, 3287. [PubMed: 31337767]

Murai J, Huang SY, Das BB, Renaud A, Zhang Y, Doroshow JH, Ji J, Takeda S, and Pommier Y (2012). Trapping of PARP1 and PARP2 by Clinical PARP Inhibitors. Cancer Res 72, 5588–5599. [PubMed: 23118055]

Murai J, Marchand C, Shahane SA, Sun H, Huang R, Zhang Y, Chergui A, Ji J, Doroshow JH, Jadhav A, et al. (2014). Identification of novel PARP inhibitors using a cell-based TDP1 inhibitory assay in a quantitative high-throughput screening platform. DNA Repair (Amst) 21, 177–182. [PubMed: 24794403]

Nacson J, Krais JJ, Bernhardy AJ, Clausen E, Feng W, Wang Y, Nicolas E, Cai KQ, Tricarico R, Hua X, et al. (2018). BRCA1 Mutation-Specific Responses to 53BP1 Loss-Induced Homologous Recombination and PARP Inhibitor Resistance. Cell Rep 25, 1384. [PubMed: 30380426]

Negrini S, Gorgoulis VG, and Halazonetis TD (2010). Genomic instability--an evolving hallmark of cancer. Nat Rev Mol Cell Biol 11, 220–228. [PubMed: 20177397]

Noordermeer SM, and van Attikum H (2019). PARP Inhibitor Resistance: A Tug of-War in BRCA-Mutated Cells. Trends Cell Biol 29, 820–834. [PubMed: 31421928]

Ogryzko VV, Schiltz RL, Russanova V, Howard BH, and Nakatani Y (1996). The transcriptional coactivators p300 and CBP are histone acetyltransferases. Cell 87, 953–959. [PubMed: 8945521]

Pettitt SJ, Rehman FL, Bajrami I, Brough R, Wallberg F, Kozarewa I, Fenwick K, Assiotis I, Chen L, Campbell J, et al. (2013). A genetic screen using the PiggyBac transposon in haploid cells identifies Parp1 as a mediator of olaparib toxicity. PLoS One 8, e61520. [PubMed: 23634208]

Porro A, Berti M, Pizzolato J, Bologna S, Kaden S, Saxer A, Ma Y, Nagasawa K, Sartori AA, and Jiricny J (2017). FAN1 interaction with ubiquitylated PCNA alleviates replication stress and preserves genomic integrity independently of BRCA2. Nat Commun 8, 1073. [PubMed: 29051491]

Quinet A, Carvajal-Maldonado D, Lemacon D, and Vindigni A (2017a). DNA Fiber Analysis: Mind the Gap! Methods Enzymol 591, 55–82. [PubMed: 28645379]

Quinet A, Lemacon D, and Vindigni A (2017b). Replication Fork Reversal: Players and Guardians. Mol Cell 68, 830–833. [PubMed: 29220651]

Rasmussen RD, Gajjar MK, Jensen KE, and Hamerlik P (2016). Enhanced efficacy of combined HDAC and PARP targeting in glioblastoma. Mol Oncol 10, 751–763. [PubMed: 26794465]

Ray Chaudhuri A, Callen E, Ding X, Gogola E, Duarte AA, Lee JE, Wong N, Lafarga V, Calvo JA, Panzarino NJ, et al. (2016). Replication fork stability confers chemoresistance in BRCA-deficient cells. Nature 535, 382–387. [PubMed: 27443740]

Rona GB, Eleutherio ECA, and Pinheiro AS (2016). PWWP domains and their modes of sensing DNA and histone methylated lysines. Biophys Rev 8, 63–74. [PubMed: 28510146]

Rondinelli B, Gogola E, Yucel H, Duarte AA, van de Ven M, van der Sluijs R, Konstantinopoulos PA, Jonkers J, Ceccaldi R, Rottenberg S, et al. (2017). EZH2 promotes degradation of stalled replication forks by recruiting MUS81 through histone H3 trimethylation. Nat Cell Biol 19, 1371–1378. [PubMed: 29035360]

Roy S, Luzwick JW, and Schlacher K (2018). SIRF: Quantitative in situ analysis of protein interactions at DNA replication forks. J Cell Biol 217, 1521–1536. [PubMed: 29475976]

Saadat N, and Gupta SV (2012). Potential role of garcinol as an anticancer agent. J Oncol 2012, 647206. [PubMed: 22745638]

Saldivar JC, Cortez D, and Cimprich KA (2017). The essential kinase ATR: ensuring faithful duplication of a challenging genome. Nat Rev Mol Cell Biol 18, 622–636. [PubMed: 28811666]

Schlacher K, Christ N, Siaud N, Egashira A, Wu H, and Jasin M (2011). Double-strand break repair-independent role for BRCA2 in blocking stalled replication fork degradation by MRE11. Cell 145, 529–542. [PubMed: 21565612]

Schlacher K, Wu H, and Jasin M (2012). A distinct replication fork protection pathway connects Fanconi anemia tumor suppressors to RAD51-BRCA1/2. Cancer Cell 22, 106–116. [PubMed: 22789542]

Shiotani B, and Zou L (2009). ATR signaling at a glance. J Cell Sci 122, 301–304. [PubMed: 19158338]

Stracker TH, and Petrini JH (2011). The MRE11 complex: starting from the ends. Nat Rev Mol Cell Biol 12, 90–103. [PubMed: 21252998]

Sun C, Yin J, Fang Y, Chen J, Jeong KJ, Chen X, Vellano CP, Ju Z, Zhao W, Zhang D, et al. (2018). BRD4 Inhibition Is Synthetic Lethal with PARP Inhibitors through the Induction of Homologous Recombination Deficiency. Cancer Cell 33, 401–416 e408. [PubMed: 29533782]

Syed A, and Tainer JA (2018). The MRE11-RAD50-NBS1 Complex Conducts the Orchestration of Damage Signaling and Outcomes to Stress in DNA Replication and Repair. Annu Rev Biochem 87, 263–294. [PubMed: 29709199]

Taglialatela A, Alvarez S, Leuzzi G, Sannino V, Ranjha L, Huang JW, Madubata C, Anand R, Levy B, Rabadan R, et al. (2017). Restoration of Replication Fork Stability in BRCA1- and BRCA2-Deficient Cells by Inactivation of SNF2-Family Fork Remodelers. Mol Cell 68, 414–430 e418. [PubMed: 29053959]

Thangavel S, Berti M, Levikova M, Pinto C, Gomathinayagam S, Vujanovic M, Zellweger R, Moore H, Lee EH, Hendrickson EA, et al. (2015). DNA2 drives processing and restart of reversed replication forks in human cells. J Cell Biol 208, 545–562. [PubMed: 25733713]

Toledo LI, Altmeyer M, Rask MB, Lukas C, Larsen DH, Povlsen LK, Bekker-Jensen S, Mailand N, Bartek J, and Lukas J (2013). ATR prohibits replication catastrophe by preventing global exhaustion of RPA. Cell 155, 1088–1103. [PubMed: 24267891]

Vujanovic M, Krietsch J, Raso MC, Terraneo N, Zellweger R, Schmid JA, Taglialatela A, Huang JW, Holland CL, Zwicky K, et al. (2017). Replication Fork Slowing and Reversal upon DNA Damage Require PCNA Polyubiquitination and ZRANB3 DNA Translocase Activity. Mol Cell 67, 882–890 e885. [PubMed: 28886337]

Xu G, Chapman JR, Brandsma I, Yuan J, Mistrik M, Bouwman P, Bartkova J, Gogola E, Warmerdam D, Barazas M, et al. (2015). REV7 counteracts DNA double-strand break resection and affects PARP inhibition. Nature 521, 541–544. [PubMed: 25799992]

Yang L, Zhang Y, Shan W, Hu Z, Yuan J, Pi J, Wang Y, Fan L, Tang Z, Li C, et al. (2017). Repression of BET activity sensitizes homologous recombination-proficient cancers to PARP inhibition. Sci Transl Med 9.

Yang SH, Zhou R, Campbell J, Chen J, Ha T, and Paull TT (2013). The SOSS1 single-stranded DNA binding complex promotes DNA end resection in concert with Exo1. EMBO J 32, 126–139. [PubMed: 23178594]

Yazinski SA, Comaills V, Buisson R, Genois MM, Nguyen HD, Ho CK, Todorova Kwan T, Morris R, Lauffer S, Nussenzweig A, et al. (2017). ATR inhibition disrupts rewired homologous recombination and fork protection pathways in PARP inhibitor-resistant BRCA-deficient cancer cells. Genes Dev 31, 318–332. [PubMed: 28242626]

Yin L, Liu Y, Peng Y, Peng Y, Yu X, Gao Y, Yuan B, Zhu Q, Cao T, He L, et al. (2018). PARP inhibitor veliparib and HDAC inhibitor SAHA synergistically co-target the UHRF1/BRCA1 DNA damage repair complex in prostate cancer cells. J Exp Clin Cancer Res 37, 153. [PubMed: 30012171]

Ying S, Hamdy FC, and Helleday T (2012). Mre11-dependent degradation of stalled DNA replication forks is prevented by BRCA2 and PARP1. Cancer Res 72, 2814–2821. [PubMed: 22447567]

Zhao J, Yang T, Ji J, Li C, Li Z, and Li L (2018). Garcinol exerts anti-cancer effect in human cervical cancer cells through upregulation of T-cadherin. Biomed Pharmacother 107, 957–966. [PubMed: 30257408]

Zhao M, Geng R, Guo X, Yuan R, Zhou X, Zhong Y, Huo Y, Zhou M, Shen Q, Li Y, et al. (2017). PCAF/GCN5-Mediated Acetylation of RPA1 Promotes Nucleotide Excision Repair. Cell Rep 20, 1997–2009. [PubMed: 28854354]

Highlights

- Loss of PCAF results in fork protection and PARPi resistance in BRCA-deficient cell

- PCAF acetylates histone H4 at lysine 8 at stalled replication forks

- MRE11 and EXO1 bind to H4K8ac at stalled replication forks in BRCA-deficient cell

- PCAF is phosphorylated by ATR at S264, which limits PCAF functions at stalled forks
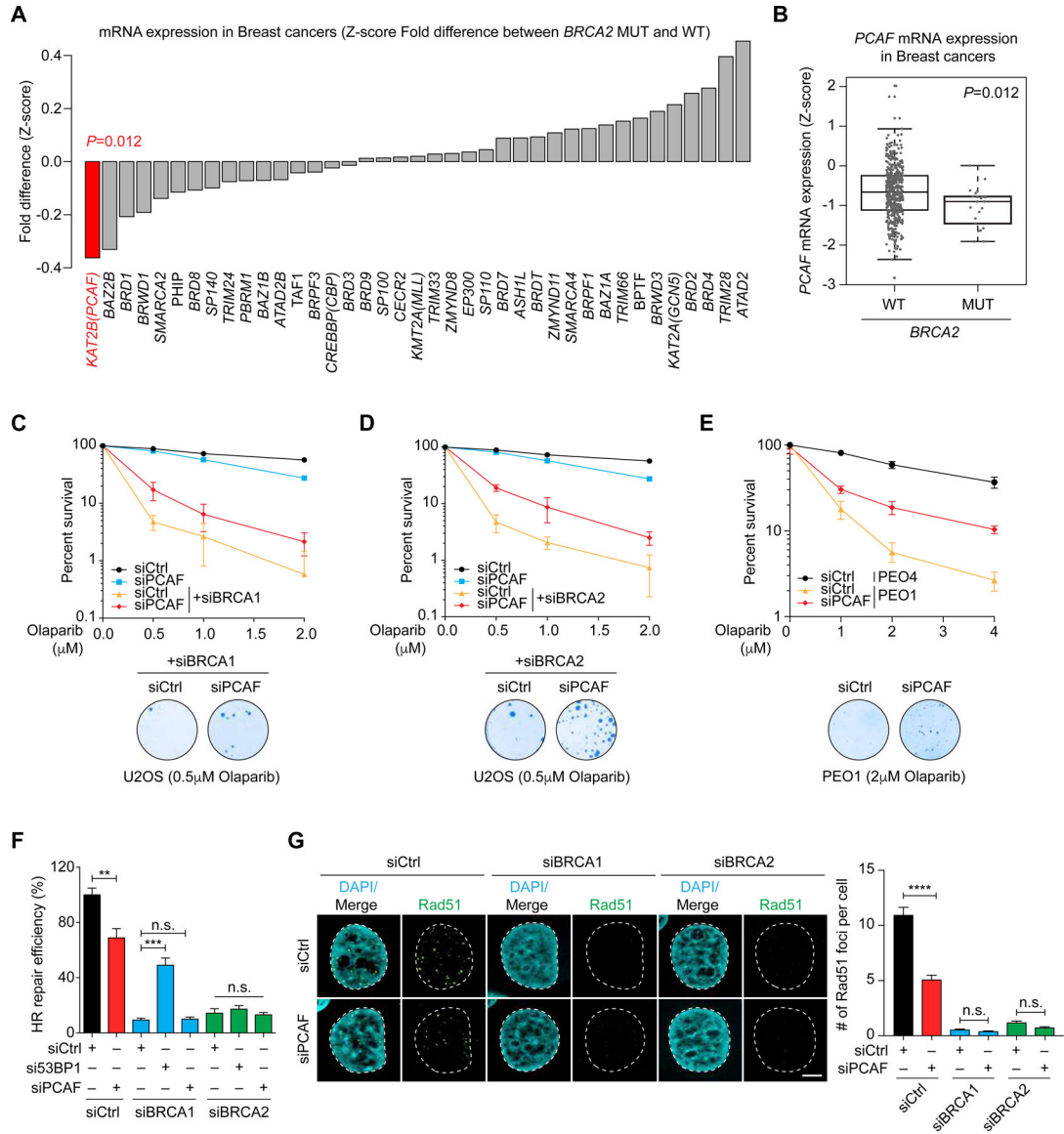
Figure 1. *PCAF* deficiency is observed in cancers and promotes PARP inhibitor resistance in *BRCA*1/2-mutated cancer cells.

(A and B) Bromodomain-containing gene expression analysis in *BRCA2*-mutated Breast cancers. (A) Barplots show the differential expression levels for the bromodomain-containing genes (n=39) between the *BRCA2* mutant (MUT, n=22) and wild-type (WT, n=459) groups in breast cancer (TCGA, (Cancer Genome Atlas, 2012)). (B) Boxplots show the *PCAF* expression levels in *BRCA2* wild-type (WT) and *BRCA2* mutant (MUT) groups in breast cancers. Statistical significances were estimated by permutated Student's *t*-test and *P*-values are indicated in the figures. (C-E) Depletion of PCAF promotes PARP inhibitor (PARPi) resistance in *BRCA1/2*-deficient cells. Clonogenic cell survival assays were performed in indicated siRNA-transfected U2OS cells (C and D) or PEO1 (*BRCA2* mutant) and PEO4 (*BRCA2* revertant) cells (E) after PARPi (Olaparib) treatment as indicated. Survival rates were normalized to control cells and plotted (representative images in lower panels). Data represent the mean ± S.D.; N=3. (F and G) PCAF depletion does not restore

HR efficiency in BRCA1/2 knockdown cells. Cells were transfected with indicated siRNAs and analyzed for HR repair efficiency (F) using DR-GFP-reporter assay or RAD51 foci formation after IR-treatment (5 Gy; G). Data represent the mean, N=3 and RAD51 foci per cell was quantified from >100 cells. ****$P < 0.0001$, *$P < 0.05$, n.s., not significant. See also Figure S1.
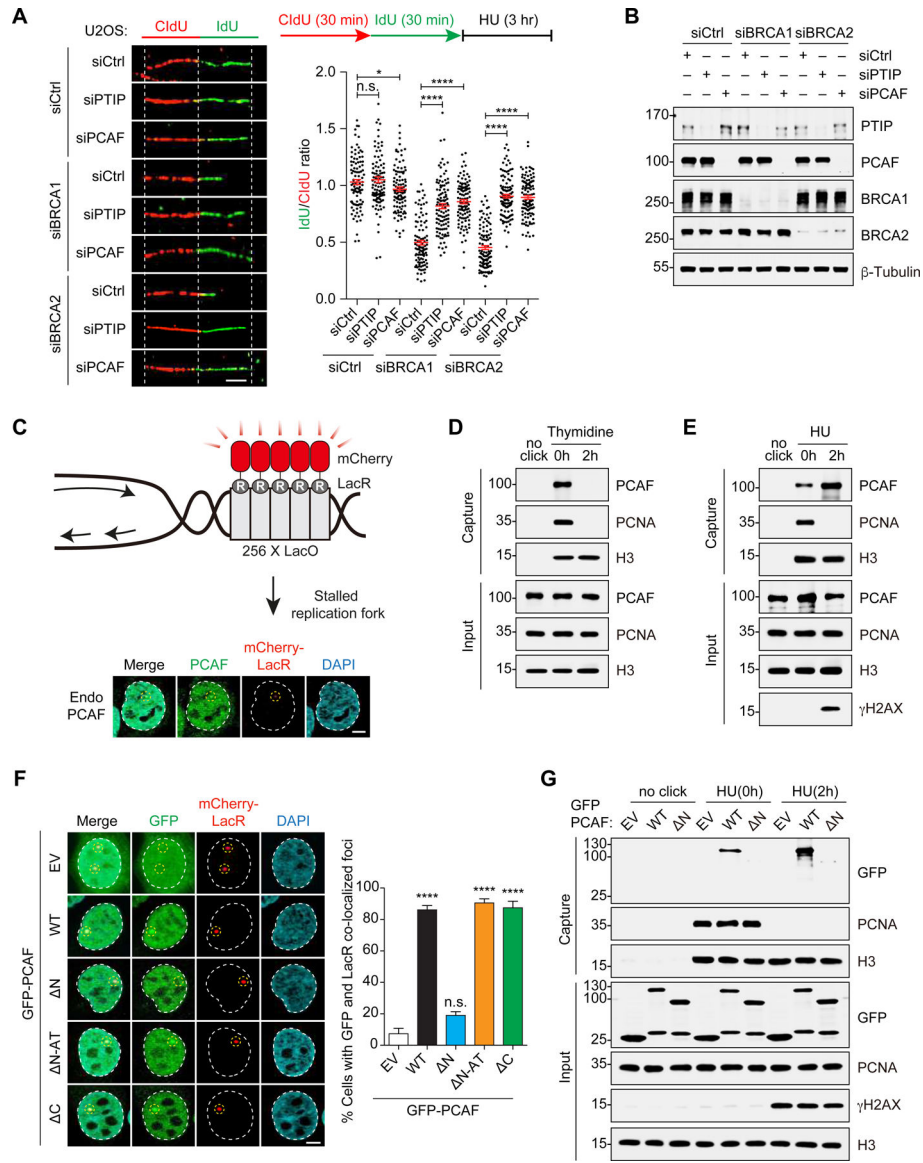
Figure 2. PCAF promotes degradation of stalled replication fork in BRCA1/2-deficient cells.
(A) DNA fiber assay. Representative fiber images for each sample are shown in left panel (quantified in right panel). U2OS cells were transfected with indicated siRNAs and then treated CIdU (30 μM), IdU (250 μM), HU (4 mM) in the order indicated. Fibers were quantified by IdU/CIdU ratio and statistical analysis performed by Mann-Whitney test. Red bar indicates mean ± S.E.M. from >100 fibers. ****$P < 0.0001$, *$P < 0.05$, n.s., not significant. (B) Knockdown efficiency of siRNAs from *A* was confirmed by western blotting. (C) PCAF localizes to stalled replication forks. Scheme for LacO array system is shown in upper panel. Endogenous PCAF localizes at LacR-induced replication lesions (lower panel). mCherry-tagged LacR was transfected into U2OS-LacO-I-SceI-TetO cells and PCAF (green) and mCherry (red) were detected by IF. (D and E) iPOND analysis of PCAF at replication forks. HEK293 cells were treated with thymidine (10 μM, 2 h; D) or HU (4 mM, 2 h; E) following EdU treatment and analysis by iPOND. H3, PCNA and

γH2AX act as experimental controls. (F and G) PCAF N-terminal domain mediates recruitment to the stalled replication forks. PCAF localization to stalled replication forks was examined by LacO array system (F) or iPOND (G) using GFP-tagged WT or mutant PCAF as indicated. For *F*, data represent the mean ± S.E.M. from >30 cells. ****$P <$ 0.0001. n.s., not significant. For *G*, HEK293 cells expressing empty vector, GFPPCAF WT or ΔN mutant were treated with HU (4 mM, 2 h) following EdU (10 μM, 15 min) treatment for iPOND analysis as in *E*. See also Figure S2.
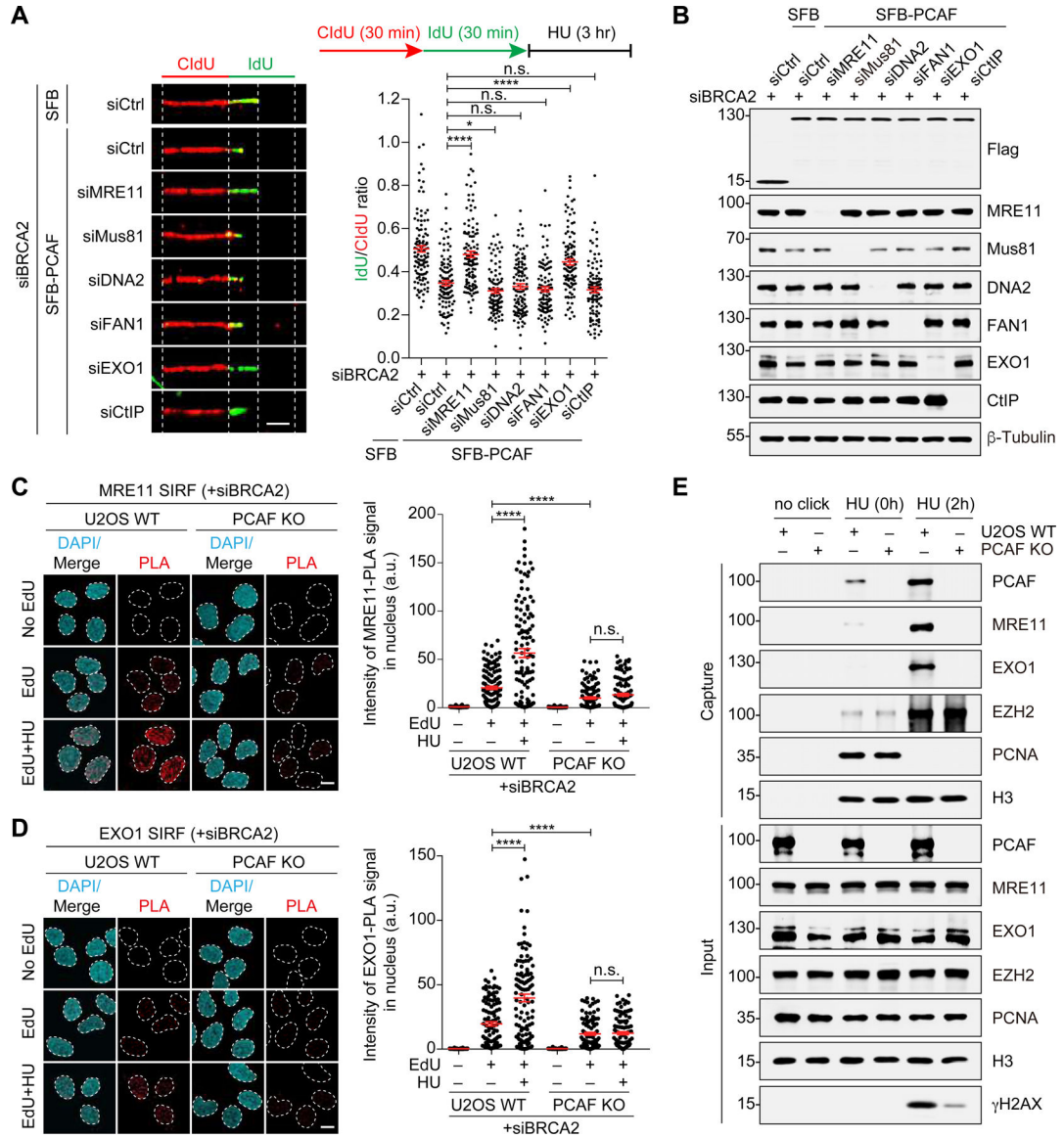
Figure 3. PCAF recruits MRE11 and EXO1 to promote degradation of stalled replication forks in BRCA2-deficient cells.

(A) MRE1 and EXO1 facilitate PCAF-mediated fork degradation in BRCA2-deficient cells. SFB-tagged PCAF was transfected into siBRCA2-depleted U2OS cells containing siRNAs targeting several DNA nucleases. DNA fiber assays were performed as in Figure 2A and analyzed by Mann-Whitney test (S.E.M. from >100 fibers). ****$P < 0.0001$, *$P < 0.05$, n.s., not significant. (B) The knockdown efficiency for siRNAs in *A* was confirmed by western blotting. (C-E) PCAF stimulates MRE11 and EXO1 recruitment to stalled replication forks. Localization of MRE11 and EXO1 was detected by SIRF assay (C and D) and iPOND (E). SIRF assay was performed in EdU-treated (125 μM, 8 min) WT and PCAF KO U2OS cells. For replication fork stalling, cells were treated with EdU prior to HU (4 mM, 3 h) treatment and analysis. Data was analyzed by Mann-Whitney test for significance. Red bars indicate mean ± S.E.M. from >100 cells. ****$P < 0.0001$, n.s., not significant (C and D). For *E*, WT and PCAF KO U2OS cells were subjected to HU (4 mM, 2 h)-induced replication stress

following EdU (10 μM, 15 min) treatment and iPOND analysis. Samples were analyzed by western blotting as in Figure 2E. See also Figure S3 and S4.
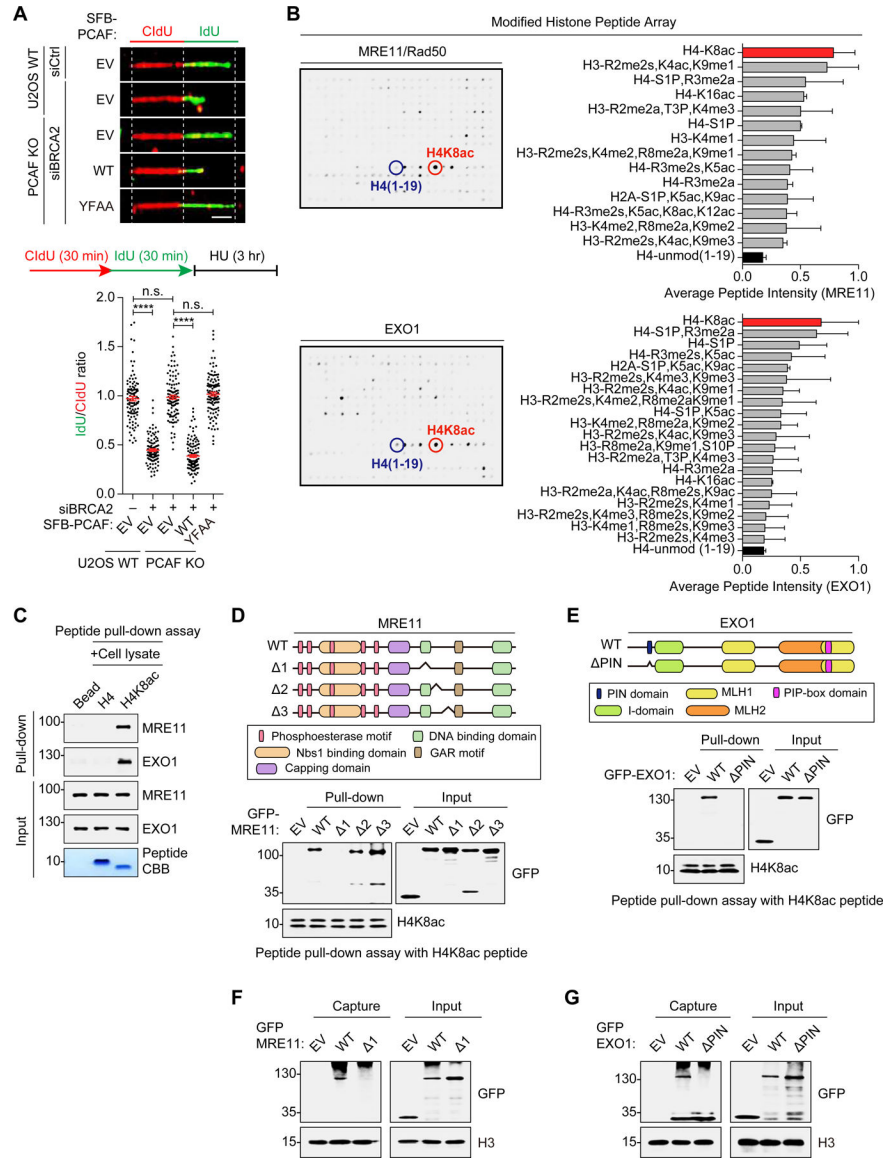
Figure 4. MRE11 and EXO1 accumulate at replication forks *via* PCAF-mediated H4K8ac.
(A) PCAF HAT activity is required for fork degradation promotion. Empty vector, SFB-tagged WT or YFAA (catalytic-dead mutant) PCAF were expressed in siBRCA2-depleted PCAF KO U2OS cells. DNA fiber assays were performed as in Figure 2. Data represent mean ± S.E.M. from >100 fibers, with statistical analysis performed using Mann-Whitney test and red bars indicate the median. ****P< 0.0001, n.s., not significant. (B) Histone peptide array analysis identifies recombinant MRE11/RAD50 and EXO1 proteins binding to acetylated histone H4 on lysine 8 (H4K8ac). Quantifications of modified peptide binding are shown in right panel (representative images in left panel, unmodified H4 is marked with blue circle and acetylated H4K8 is marked with red circle). (C) Endogenous MRE11 and EXO1 interact with acetylated H4K8 peptides. Peptide pull-down assays were performed in HEK293 cell extracts using biotinylated H4 or H4K8ac peptides. Samples were analyzed by western blotting and input peptides detected by Coomassie Brilliant Blue staining. (D and E)

Identification of H4K8ac binding region in MRE11 and EXO1. Diagram of MRE11 and EXO1 mutants are shown in upper panels and results shown in lower panels. GFP-tagged WT and mutants of MRE11 (D) or EXO1 (E) were expressed into HEK293 and peptide pull-down assays were performed as in *C*. (F and G) H4K8ac-binding regions within MRE11 and EXO1 promote recruitment to stalled replication forks. GFP-tagged MRE11 (F) and EXO1 (G) mutants recruitment were analyzed by iPOND as in Figure 2G. See also Figure S5 and S6.
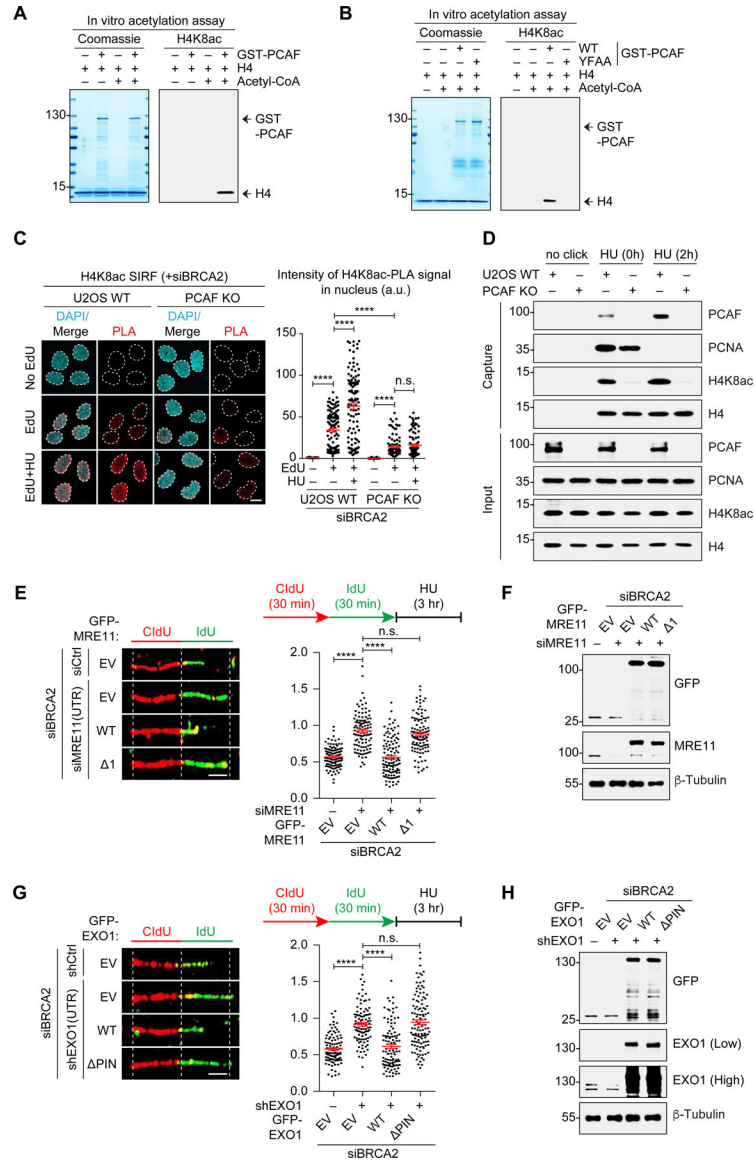
Figure 5. PCAF promotes H4K8 acetylation at the replication fork.
(A and B) PCAF acetylates H4K8 in a HAT activity dependent manner. *In vitro* acetylation assays were performed with GST-tagged PCAF and free histone H4. Acetylated H4K8 was detected by western blotting using a H4K8ac-specific antibody. The amounts of GST-PCAF and H4 peptide were confirmed by Coomassie Brilliant Blue staining in input samples. The PCAF catalytic-dead mutant (YFAA) was unable to acetylate H4K8 *in vitro*. (C and D) PCAF acetylates H4K8 at replication forks. Acetylated H4K8 levels at replication forks were detected by SIRF assay (C) and iPOND (D) in WT and PCAF KO U2OS cells. SIRF assays and iPOND analyses were performed as in Figure 3. For SIRF assay, data was analyzed by Mann-Whitney test for significance. Red bars indicate mean ± S.E.M. from >100 cells. ****P < 0.0001, n.s., not significant. (E-H). DNA fiber assays were performed in MRE11 (E) and EXO1 (G) WT or H4K8ac-binding mutant reconstituted cells. U2OS cells were transfected with siMRE11 (3'-UTR) or shEXO1 (3'-UTR) and siBRCA2, with

indicated GFP-tagged MRE11 or EXO1 derivatives expressed. DNA fibers were quantified as in Figure 2A. Data represent the mean ± S.E.M. from >100 fibers, following the Mann-Whitney test. The red bars indicate the median. ****P< 0.0001, n.s., not significant. Transfection efficiency was confirmed by western blotting (F and H). See also Figure S7.
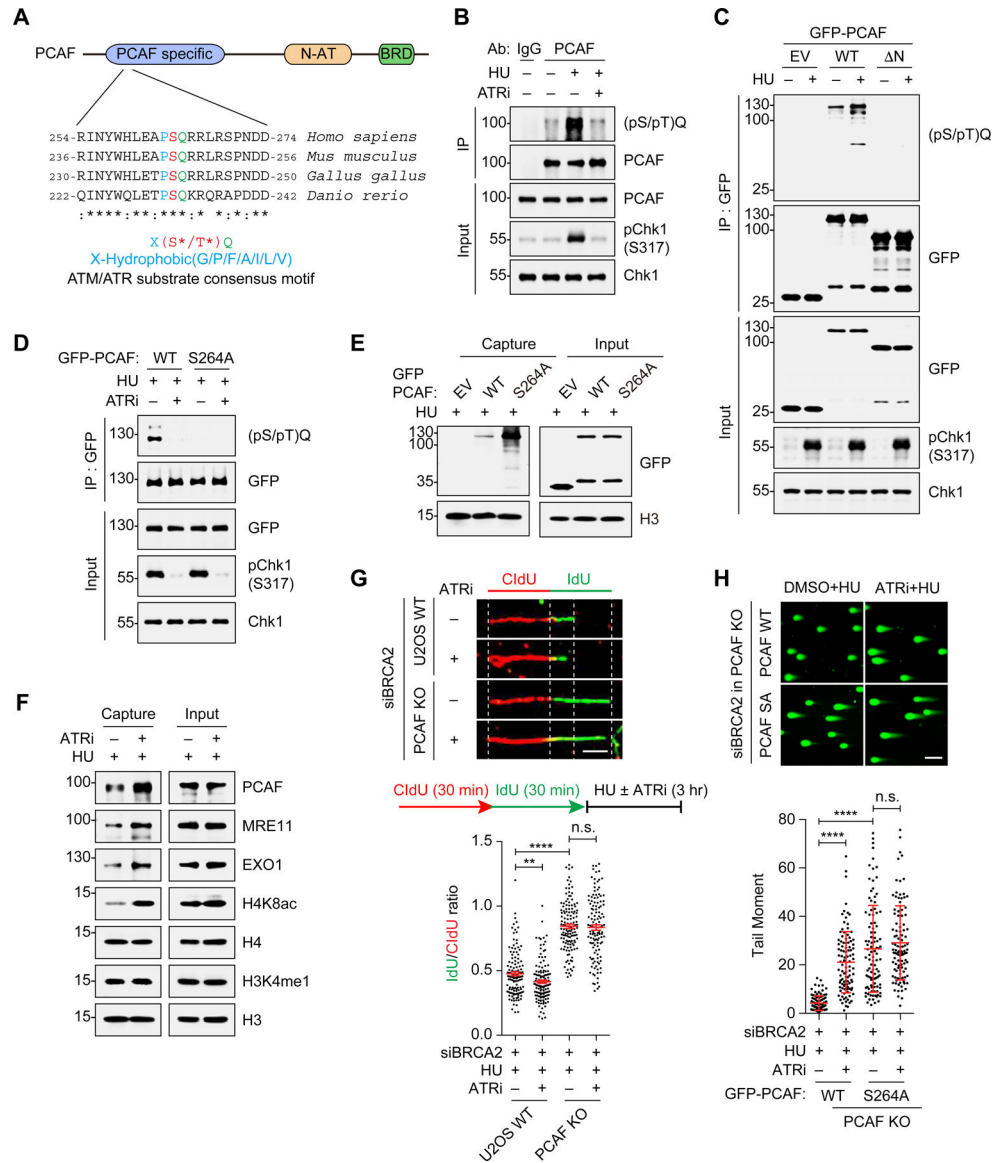
Figure 6. ATR phosphorylates PCAF to prevent excessive fork degradation and DSBs formation.
(A) PCAF domain structure and identification of a highly conserved ATM/ATR SQ consensus motif within the N-terminal region at serine 264. (B-D) PCAF S264 is phosphorylated by ATR. Endogenous PCAF was IPed in HEK293 cells treated with mock or HU (4 mM, 2 h). Phosphorylated-PCAF was detected by western blot with a phospho-(S/T)Q specific antibody, which required ATR (B) and occurred on S264 in N terminal domain (C and D). ATR inhibitor (5 μM, 16 h) and further HU (4 mM) + ATRi (5 μM) treatments (2 h) were performed before analysis. IgG was used as experimental control and ATR inhibitor activity was confirmed by anti-pCHK1 (S317) blot. For *C*, GFP-tagged PCAF WT or ΔN were analyzed by IP with GFP-Trap bead in HU-treated (4 mM, 2 h) HEK293 cells. For *D*, GFP-PCAF WT or S264A mutants were analyzed as in *C*. (E) ATR controls PCAF recruitment to the replication forks through S264 phosphorylation. HEK293 cells expressing empty vector, WT or S264A GFP-PCAF were analyzed by iPOND in HU-treated

conditions. Cells were analyzed as in *C*. PCAF was detected by western blot with anti-GFP antibody, and anti-H3 was used as experimental control. (F and G) ATR constrains PCAF and fork degradation at stalled replication forks in BRCA2-deficient cells. In *F*, PCAF-mediated H4K8ac and MRE11/EXO1 recruitments were analyzed by iPOND −/+ ATR inhibitor (5 μM, 18 h) in HEK293 cells. In *G*, DNA fiber assays were performed −/+ ATR inhibitor (5 μM, 3 h) in WT and PCAF KO U2OS cells. Cells were transfected with siBRCA2 and treated with CIdU (30 μM), IdU (250 μM), HU (4 mM; HU+DMSO or HU +ATRi) as indicated. DNA fibers were quantified as in Figure 2A. Data represent the mean ± S.E.M. from >100 fibers, following the Mann-Whitney test. The red bars indicate the median. ****$P < 0.0001$, **$P < 0.01$, n.s., not significant. (H) PCAF-S264 phosphorylation by ATR prevents excessive DSBs formation in HU-treated cells. GFP-tagged PCAF WT and S264A mutant were co-transfected with siBRCA2 into PCAF KO cells. DSBs levels were measured by neutral comet assay in the presence or absence of ATR inhibitor (5 μM, 2 h; lower panel). Data represent the mean ± S.E.M. from >100 cells by Mann-Whitney test and red bars indicate the median. ****$P < 0.0001$, n.s., not significant.
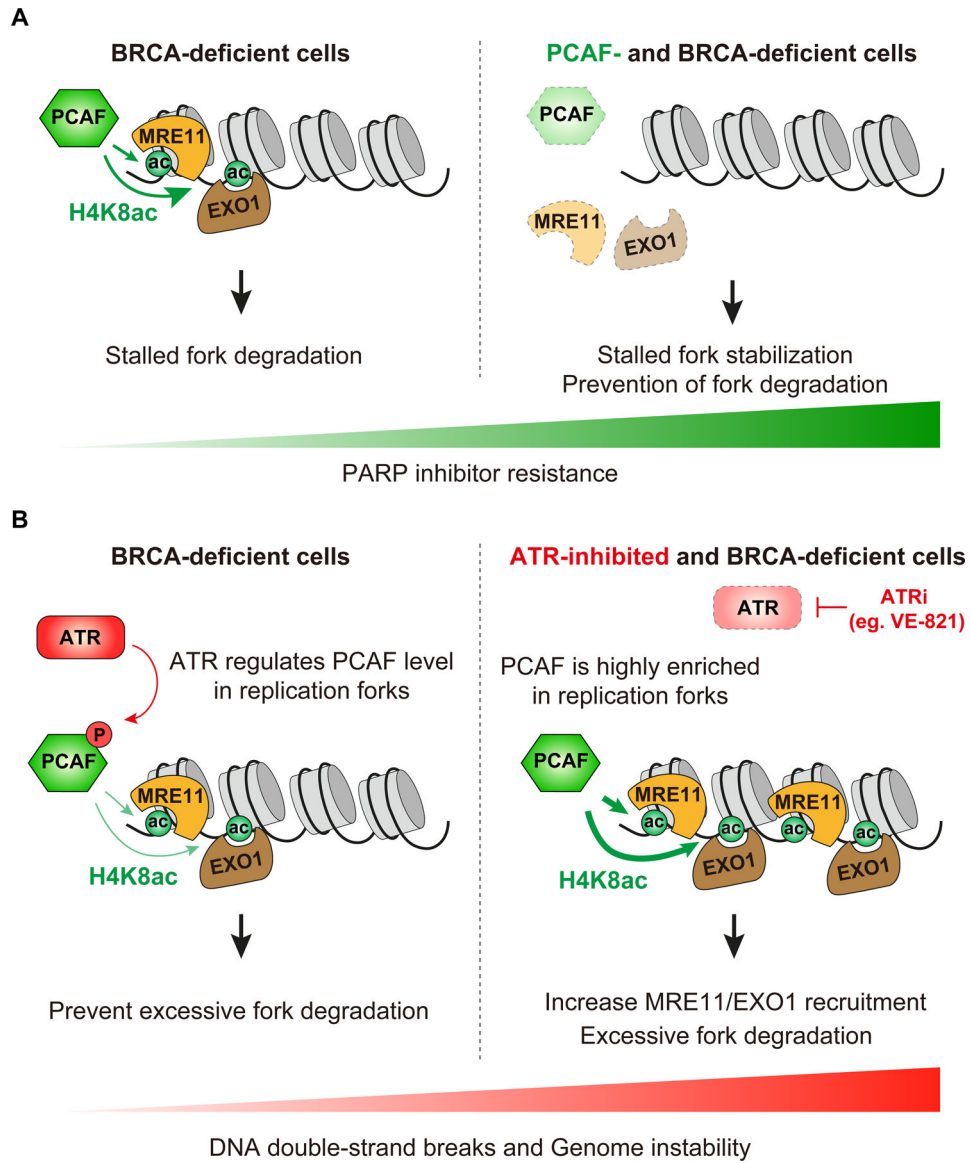
Figure 7. Model for PCAF mediated replication fork processing in BRCA-deficient cells.
(A) PCAF localizes to stalled replication forks and acetylates histone H4K8, which facilitates MRE11 and EXO1 recruitment to promote fork degradation in BRCA-deficient cells. (B) The replication stress kinase ATR phosphorylates PCAF on S264 to limit its activity at replication forks, constraining fork degradation and DSBs. Upon ATR inhibition, PCAF is enriched at replication forks which facilitates fork degradation and DSBs.

KEY RESOURCES TABLE

REAGENT or RESOURCE	SOURCE	IDENTIFIER
Antibodies		
Anti-PCAF (C14G9) Antibody	Cell Signaling	Cat# 3378S
Anti-KAT2B/PCAF Antibody (For IP)	Abcam	Cat# ab12188
Anti-Rad51 Antibody	GeneTex	Cat# GTX100469
Anti-PTIP Antibody	Bethyl	Cat# A300-370A
Anti-BRCA1 Antibody	Millipore	Cat# 07-434
Anti-BRCA2 Antibody	Abcam	Cat# ab27976
Anti-53BP1 Antibody	Novus Biologicals	Cat# NB100-304
Anti-MRE11 Antibody	Novus Biologicals	Cat# NB100-142
Anti-Mus81 Antibody	Abcam	Cat# ab14387
Anti-DNA2 Antibody	Abcam	Cat# ab96488
Anti-FAN1 Antibody	Abcam	Cat# ab68572
Anti-CtIP Antibody	Cell Signaling	Cat# 9201S
Anti-Exonuclease 1 Antibody (For WB)	Bethyl Laboratories	Cat# A302-640A
Anti-Exonuclease 1 Antibody (For SIRF)	GeneTex	Cat# GTX109891
Anti-EZH2 (D2C9) Antibody	Cell Signaling	Cat# 5246T
Anti-Beta Tubulin Antibody	Abcam	Cat# ab6046
Anti-Histone H3 Antibody	Abcam	Cat# ab1791
Anti-Histone H4 Antibody	Abcam	Cat# ab7311
Anti-Histone H3K4me1 Antibody	Active motif	Cat# 61633
Anti-Histone H3K4me3 Antibody	Abcam	Cat# ab8580
Anti-acetyl-Histone H4 (Lys8) Antibody	Millipore	Cat# 07-328
Anti-phospho Histone H2A.X (Ser139) Antibody	Millipore	Cat# 05-636-AF647
Anti-GFP Antibody	Abcam	Cat# ab290
Anti-mCherry (Rabbit) Antibody	Abcam	Cat# ab167453
Anti-mCherry (Mouse) Antibody	Millipore	Cat# MAB131873
Anti-PCNA Antibody	Abcam	Cat# ab18197
Anti-Chk1 Antibody	Santa Cruz	Cat# sc-8408
Anti-phospho Chk1 (Ser317) Antibody	Cell Signaling	Cat# 2344S
Anti-phospho-(Ser/Thr) ATM/ATR Substrate Antibody	Cell Signaling	Cat# 2851S
Anti-BrdU(Mouse) Antibody (clone B44)	BD Biosciences	Cat# 347580
Anti-BrdU(Rat) Antibody [BU1/75 (ICR1)]	Abcam	Cat# ab6326
Anti-Biotin Antibody (clone BN-34)	Sigma-Aldrich	Cat# B7653
Anti-SMARCAL1 Antibody	Bethyl Laboratories	Cat# A301-616A
Anti-HLTF Antibody	Abcam	Cat# ab17984
Anti-ZRANB3 Antibody	Sigma-Aldrich	Cat# HPA035234
Anti-Normal Rabbit IgG	Calbiochem	Cat# NI01

REAGENT or RESOURCE	SOURCE	IDENTIFIER
Anti-mouse IgG, HRP-linked Antibody	Cell Signaling	Cat# 7076S
Anti-rabbit IgG, HRP-linked Antibody	Cell Signaling	Cat# 7074S
Alexa Fluor 488 goat anti-mouse IgG	Invitrogen	Cat# A-11029
Alexa Fluor 594 goat anti-mouse IgG	Invitrogen	Cat# A-11032
Alexa Fluor 488 goat anti-rabbit IgG	Invitrogen	Cat# A-11034
Alexa Fluor 594 goat anti-rabbit IgG	Invitrogen	Cat# A-11037
Alexa Fluor 594 goat anti-rat IgG	Invitrogen	Cat# A-11007
Bacterial and Virus Strains		
One Shot™ TOP10™ chemically Competent *E. coli*	Invitrogen	Cat# C404003
BL21 (DE3) Competent Cells	Thermo Scientific	Cat# EC0114
Chemicals, Peptides, and Recombinant Proteins		
Lipofectamine 2000	Invitrogen	Cat# 11668027
Lipofectamine RNAiMax	Invitrogen	Cat# 13778075
Polyethylenimine	Polysciences	Cat# 24314-2
5-Chloro-2′-deoxyuridine (CIdU)	Sigma-Aldrich	Cat# C6891
5-Iodo-2′-deoxyuridine (IdU)	Sigma-Aldrich	Cat# I7125
5-bromo-2'-deoxyuridine (BrdU)	Sigma-Aldrich	Cat# B9285
Hydroxyurea (HU)	Sigma-Aldrich	Cat# H8627
Hexadimethrine bromide (Polybrene)	Sigma-Aldrich	Cat# 107689
VE-821 (ATR inhibitor)	Selleckchem	Cat# S8007
Gateway™ LR Clonase™ II Enzyme Mix	Invitrogen	Cat# 11791100
Q5 High-Fidelity DNA polymerase	New England Biolabs	Cat# M0491L
Q5 Hot start High-Fidelity 2X Master Mix	New England Biolabs	Cat# M0492L
KLD Enzyme Mix	New England Biolabs	Cat# M0554S
Crystal Violet	Sigma-Aldrich	Cat# C3886
VECTASHIELD® Mounting Medium with DAPI	Vector Labs	Cat# H-1200
Dynabeads™ MyOne™ Streptavidin T1	Invitrogen	Cat# 65602
GFP-Trap®_MA	ChromoTek	Cat# gtma-20
Dynabeads® Protein A	Invitrogen	Cat# 10002D
Dynabeads® Protein G	Invitrogen	Cat# 100040
Peptide: [Lys(Ac)8] Histone H4(1-25) - biotin labeled	AnaSpec	Cat# AS-65230-1
Peptide: Histone H4 (1-25) - biotin labeled	AnaSpec	Cat# AS-65242-1
Recombinant Protein: PCAF WT	This paper	N/A
Recombinant Protein: PCAF YFAA	This paper	N/A
Recombinant Protein: MRE11/Rad50	Dr. Tanya T. Paull	(Yang et al., 2013)
Recombinant Protein: EXO1	Dr. Tanya T. Paull	(Yang et al., 2013)
Critical Commercial Assays		
Click-iT™ EdU Alexa Fluor™ 647 Imaging Kit	Invitrogen	Cat# C10340
Duolink® In Situ PLA® Probe Anti-Rabbit PLUS	Sigma-Aldrich	Cat# DUO92002

REAGENT or RESOURCE	SOURCE	IDENTIFIER
Duolink® In Situ PLA® Probe Anti-Mouse MINUS	Sigma-Aldrich	Cat# DUO92004
Duolink® In Situ Detection Reagents Red	Sigma-Aldrich	Cat# DUO92008
QuikChange II Site-Directed Mutagenesis Kit	Agilent Technologies	Cat# 200523
Deposited Data		
Original Raw data	Mendeley Data; this study	https://data.mendeley.com/datasets/35wphpgv48/draft?a=280018b1-e154-4d2f-b054-e9b19fa00753
Breast cancer dataset	(Cancer Genome Atlas, 2012)	https://www.cbioportal.org/
Ovarian cancer dataset	TCGA GDC Portal	https://portal.gdc.cancer.gov
Experimental Models: Cell Lines		
Human: U2OS	ATCC	Cat# HTB-96
Human: U2OS_PCAF KO	Our lab	(Kim et al., 2019)
Human: U2OS-DR-GFP	Dr. Jeremy M. Stark	(Gunn et al., 2011)
Human: U2OS-LacO-I-SceI-TetO	Dr. Tom Misteli	(Burgess et al., 2014)
Human: HEK293	ATCC	Cat# CRL-1573
Human: HEK293_shCtrl	This paper	N/A
Human: HEK293_shPCAF	This paper	N/A
Human: PEO1	Sigma-Aldrich	Cat# 10032308
Human: PEO4	Sigma-Aldrich	Cat# 10032309
Human: T47D	ATCC	Cat# HTB-133
Human: MCF7	ATCC	Cat# HTB-22
Human: MDA-MB-231	ATCC	Cat# HTB-26
Human: MDA-MB-436	Dr. Blerta Xhemalce	ATCC, Cat# HTB-130
Human: BT474	ATCC	Cat# HTB-20
Human: BT549	ATCC	Cat# HTB-122
Human: HCC1395	Dr. Blerta Xhemalce	ATCC, Cat# CRL-2324
Human: HCC38	Dr. Blerta Xhemalce	ATCC, Cat# CRL-2314
Human: HCC70	Dr. Blerta Xhemalce	ATCC, Cat# CRL-2315
Human: HCC1143	Dr. Blerta Xhemalce	ATCC, Cat# CRL-2321
Human: HCC1187	Dr. Blerta Xhemalce	ATCC, Cat# CRL-2322
Human: HCC1599	Dr. Blerta Xhemalce	ATCC, Cat# CRL-2331
Human: HCC1806	Dr. Blerta Xhemalce	ATCC, Cat# CRL-2335
Human: HCC1937	Dr. Blerta Xhemalce	ATCC, Cat# CRL-2336
Human: BT20	Dr. Blerta Xhemalce	ATCC, Cat# HTB-19
Human: Hs 578T	Dr. Blerta Xhemalce	ATCC, Cat# HTB-126
Human: DU4475	Dr. Blerta Xhemalce	ATCC, Cat# HTB-123
Human: MDA-MB-157	Dr. Blerta Xhemalce	ATCC, Cat# HTB-24
Human: MDA-MB-453	Dr. Blerta Xhemalce	ATCC, Cat# HTB-131
Human: MDA-MB-468	Dr. Blerta Xhemalce	ATCC, Cat# HTB-132
Oligonucleotides		
Primers used in this study, see Table S1	This paper	N/A

REAGENT or RESOURCE	SOURCE	IDENTIFIER
siRNAs/shRNAs used in this study, see Table S2	This paper	N/A
Recombinant DNA		
SFB control vector	Our lab	(Gong et al., 2015)
pcDNA6.2 N-EmGFP control vector	Our lab	(Kim et al., 2019)
N-SFB-PCAF WT	Our lab	(Kim et al., 2019)
N-SFB-PCAF N-term (1-320)	Our lab	(Kim et al., 2019)
N-SFB-PCAF N-AT (503-651)	Our lab	(Kim et al., 2019)
N-SFB-PCAF C-term (740-832)	Our lab	(Kim et al., 2019)
pcDNA6.2 N-EmGFP-PCAF WT	Our lab	(Kim et al., 2019)
pcDNA6.2 N-EmGFP-PCAF S264A	This paper	N/A
pcDNA6.2 N-EmGFP-PCAF YF(616,617)AA	Our lab	(Kim et al., 2019)
pcDNA6.2 N-EmGFP-MRE11 WT	This paper	N/A
pcDNA6.2 N-EmGFP-MRE11 F1 (1-641)	This paper	N/A
pcDNA6.2 N-EmGFP-MRE11 F2 (1-555)	This paper	N/A
pcDNA6.2 N-EmGFP-MRE11 F3 (1-406)	This paper	N/A
pcDNA6.2 N-EmGFP-MRE11 1 (407-421)	This paper	N/A
pcDNA6.2 N-EmGFP-MRE11 2 (429-482)	This paper	N/A
pcDNA6.2 N-EmGFP-MRE11 3 (483-555)	This paper	N/A
pcDNA6.2 N-EmGFP-EXO1 WT	This paper	N/A
pcDNA6.2 N-EmGFP-EXO1 WT F1 (1-785)	This paper	N/A
pcDNA6.2 N-EmGFP-EXO1 WT F2 (1-598)	This paper	N/A
pcDNA6.2 N-EmGFP-EXO1 WT F3 (1-387)	This paper	N/A
pcDNA6.2 N-EmGFP-EXO1 WT F4 (1-137)	This paper	N/A
pcDNA6.2 N-EmGFP-EXO1 WT PIN (125-135)	This paper	N/A
pMD2.G (envelope plasmid)	Dr. Roger A. Greenberg	N/A
psPAX2 (packaging plasmid)	Dr. Roger A. Greenberg	N/A
pCAG-I-SceI (I-SceI)	Dr. Jeremy M. Stark	(Gunn et al., 2011)
mCherry-LacR	Dr. Tom Misteli	(Burgess et al., 2014)
Software and Algorithms		
ImageJ (v1.48)	NIH	RRID:SCR_003070 https://imagej.nih.gov/ij/
Prism (v6)	GraphPad	RRID:SCR_002798 https://www.graphpad.com
FV-10-ASW3.1	Olympus	https://www.olympus-ims.com/en/
R package (v.3.6.1)	R Project for Statistical Computing	RRID:SCR_001905 https://www.r-project.org/